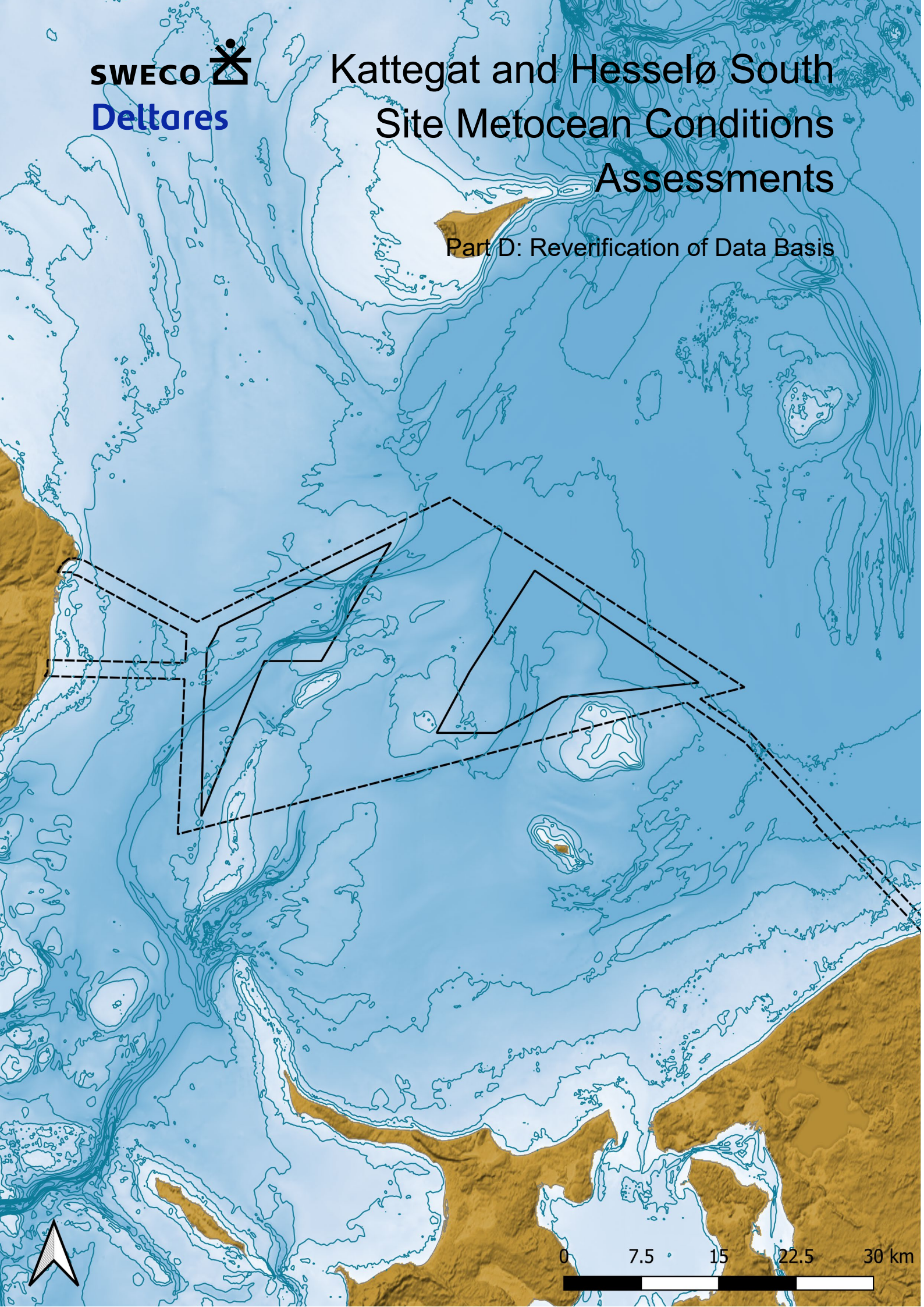


Kattegat and Hesselø South Site Metocean Conditions Assessments

Part D: Reverification of Data Basis



Change list

Ver	Date	Description of the change	Author	Reviewed	Approved by
1	2024-11-15	New Document	Bas Reijmerink, Maria Georgiou	Sofia Caires	Jan-Joost Schouten
2	2024-12-04	Revised, final version	Bas Reijmerink, Maria Georgiou	Sofia Caires	Jan-Joost Schouten
					

Project Name MetOcean Assessment for Kattegat and Hesselø South
Project Manager Anders Helkjær, anders.helkjaer@sweco.dk, +4527233341
Client Energinet Eltransmission A/S
Author Bas Reijmerink and Maria Georgiou
Controlled by Sofia Caires
Approved by Jan-Joost Schouten
Date 2024-12-04
Ver 2
Document number 41011328D
Document reference 41011328D_KGHS_PartD_Reverification_of_Data_Basis

Table of contents

1	Summary	10
2	Introduction	11
	2.1 Background	11
	2.2 Objectives	12
	2.3 Approach	12
3	Overview of measurement campaign data	13
	3.1 Introduction	13
	3.2 Kattegat measurement campaign	14
	3.3 Hesselø South measurement campaign	14
4	Wind reverification	16
	4.1 Introduction	16
	4.2 Kattegat wind	16
	4.3 Hesselø South wind	19
5	Water level reverification	23
	5.1 Introduction	23
	5.2 Kattegat water level	23
	5.3 Hesselø South water level	26
6	Current reverification	29
	6.1 Introduction	29
	6.2 Kattegat currents	29
	6.3 Hesselø South currents	37
7	Temperature reverification	44
	7.1 Kattegat and Hesselø South water temperature	44
8	Wave reverification	45
	8.1 Introduction	45
	8.2 Kattegat waves	45
	8.3 Hesselø South waves	47
9	References	50
Appendix A Error statistics		51
	Introduction	51
	Linear variables	51
	Circular variables	51
	References	53

List of Figures

Figure 2-1 Overview map of the windfarm areas Kattegat and Hesselø. The dashed line indicates the full data delivery area, and the full line indicate the OWFs. 11

Figure 3-1 Instrument locations in the Kattegat and Hesselø project area. Figure taken from Fugro (2024a). 13

Figure 4-1 Timeseries comparisons between the calibrated model results and the observations from KG-1-LB of 10 m wind speed (top panel) and direction (bottom panel). The vertical line indicates the date until which the observation data have been considered in the Deltares (2024). 17

Figure 4-2 Density scatter comparisons between the calibrated model results and the observations from KG-1-LB of 10 m wind speed (top row) and direction (bottom row). The KG-1-LB wind speed observations at 12 mMSL were converted to 10 mMSL. The periods covered by the data are 07-2023 to 02-2024 (left column), 02-2024 to 07-2024 (middle column) and 07-2023 to 07-2024 (right column). 18

Figure 4-3 Timeseries comparisons between the calibrated model results and the observations from KG-1-LB of 150 mMSL wind speed (top panel) and direction (bottom panel). The vertical line indicates the date until which the observation data have been considered in the Deltares (2024). 18

Figure 4-4 Density scatter comparisons between the calibrated model results and the observations from KG-1-LB of 150 mMSL wind speed (top row) and direction (bottom row). The periods covered by the data are 07-2023 to 02-2024 (left column), 02-2024 to 07-2024 (middle column) and 07-2023 to 07-2024 (right column). 19

Figure 4-5 Timeseries comparisons between the calibrated model results and the observations from HS-1-LB of 10 m wind speed (top panel) and direction (bottom panel). The vertical line indicates the date until which the observation data have been considered in the Deltares (2024). 20

Figure 4-6 Density scatter comparisons between the calibrated model results and the observations from HS-1-LB of 10 m wind speed (top row) and direction (bottom row). The HS-1-LB wind speed observations at 12 mMSL were converted to 10 mMSL. The periods covered by the data are 07-2023 to 02-2024 (left column), 02-2024 to 07-2024 (middle column) and 07-2023 to 07-2024 (right column). 21

Figure 4-7 Timeseries comparisons between the calibrated model results and the observations from HS-1-LB of 150 mMSL wind speed (top panel) and direction (bottom panel). The vertical line indicates the date until which the observation data have been considered in the Deltares (2024). 21

Figure 4-8 Density scatter comparisons between the calibrated model results and the observations from HS-1-LB of 150 mMSL wind speed (top row) and direction (bottom row). The periods covered by the data are 07-2023 to 02-2024 (left column), 02-2024 to 07-2024 (middle column) and 07-2023 to 07-2024 (right column). 22

Figure 5-1 Timeseries comparisons between the calibrated model results and the observations from KG-1-LB (top) and KG-1-CP (bottom) of total water level. 24

Figure 5-2 Density scatter comparisons between the calibrated 3D model results and the observations from KG-1-LB water level. The plot in the top row is for the observations received during the study, the plots in the bottom row are for the final campaign observations. The periods covered by the data are 07-2023 to 02-2024 (left column), 02-2024 to 07-2024 (middle column) and 07-2023 to 07-2024 (right column). 25

Figure 5-3 Density scatter comparisons between the calibrated 3D model results and the observations from KG-1-CP water level. The plot in the top row is for the observations received during the study, the plots in the bottom row are for the final campaign observations. The periods covered by the data are 07-2023 to 02-2024 (left column), 02-2024 to 07-2024 (middle column) and 07-2023 to 07-2024 (right column). 26

Figure 5-4 Timeseries comparisons between the calibrated model results and the observations from HS-1-LB (top) and HS-1-CP (bottom) of total water level. 27

Figure 5-5 Density scatter comparisons between the calibrated 3D model results and the observations from HS-1-LB water level water level from 04-2024 until 07-2024. 27

Figure 5-6 Density scatter comparisons between the calibrated 3D model results and the observations from HS-1-CP water level. The plot in the top row is for the observations received during the study, the plots in the bottom row are for the final campaign observations. The periods covered by the data are 07-2023 to 03-2024 (left column), 03-2024 to 07-2024 (middle column) and 07-2023 to 07-2024 (right column). 28

Figure 6-1 Timeseries comparisons between the calibrated model results and the observations from KG-1-LB (top) and KG-1-CP (bottom) of depth-averaged current speed. 30

Figure 6-2 Density scatter comparisons between the calibrated 3D model results and the observations from KG-1-LB of depth-averaged current speed. The plot in the top row is for the observations considered in Deltares (2024), the plots in the bottom row are for the final campaign observations. The periods covered by the data are 07-2023 to 02-2024 (left column), 02-2024 to 07-2024 (middle column) and 07-2023 to 07-2024 (right column). 31

Figure 6-3 Density scatter comparisons between the calibrated 3D model results and the observations from KG-1-CP of depth-averaged current speed. The plot in the top row is for the observations considered in Deltares (2024), the plots in the bottom row are for the final campaign observations. The periods covered by the data are 07-2023 to 02-2024 (left column), 02-2024 to 07-2024 (middle column) and 07-2023 to 07-2024 (right column). 32

Figure 6-4 Current speed Hovmöller diagrams of the calibrated model results and the observations from KG-1-LB. The plot in the top row is with the observations considered in Deltares (2024), the plot in the bottom row is with the final campaign observations and the plot in the bottom row is with the model results. 33

Figure 6-5 Current magnitude 3D profile plots comparisons between the calibrated 3D model results (dashed lines) and the observations (full lines) from KG-1-LB. The plot in the top row is for the observations considered in Deltares (2024), the plots in the bottom row are for the final campaign observations. The periods covered by the data are 07-2023 to 03-2024 (left column), 03-2024 to 07-2024 (middle column) and 07-2023 to 07-2024 (right column). 34

Figure 6-6 Current speed Hovmöller diagrams of the calibrated model results and the observations from KG-1-CP. The plot in the top row is with the observations considered in Deltares (2024), the plot in the bottom row is with the final campaign observations and the plot in the bottom row is with the model results. 35

Figure 6-7 Current magnitude 3D profile plots comparisons between the calibrated 3D model results (dashed lines) and the observations (full lines) from KG-1-CP. The plot in the top row is for the observations considered in Deltares (2024), the plots in the bottom row are for the final campaign observations. The periods covered by the data are 07-2023 to 03-2024 (left column), 03-2024 to 07-2024 (middle column) and 07-2023 to 07-2024 (right column). 36

Figure 6-8 Timeseries comparisons between the calibrated model results and the observations from HS-1-LB (top) and HS-1-CP (bottom) of depth-averaged current speed. 37

Figure 6-9 Density scatter comparisons between the calibrated 3D model results and the observations from HS-1-LB of depth-averaged current speed. The plot in the top row is for the observations considered in Deltares (2024), the plots in the bottom row are for the final campaign observations. The periods covered by the data are 07-2023 to 02-2024 (left column, no valid data in the final campaign dataset), 02-2024 to 07-2024 (middle column) and 07-2023 to 07-2024 (right column). 38

Figure 6-10 Density scatter comparisons between the calibrated 3D model results and the observations from HS-1-CP of depth-averaged current speed. The plot in the top row is for the observations considered in Deltares (2024), the plots in the bottom row are for the final campaign observations. The periods covered by the data are 07-2023 to 03-2024 (left column), 03-2024 to 07-2024 (middle column) and 07-2023 to 07-2024 (right column). 39

Figure 6-11 Current speed Hovmöller diagrams of the calibrated model results and the observations from HS-1-LB. The plot in the top row is with the observations considered in Deltares (2024), the plot in the bottom row is with the final campaign observations and the plot in the bottom row is with the model results..... 40

Figure 6-12 Current magnitude 3D profile plots comparisons between the calibrated 3D model results (dashed lines) and the observations (full lines) from HS-1-LB. The plot in the top row is for the observations considered in Deltares (2024), the plots in the bottom row are for the final campaign observations. The periods covered by the data are 07-2023 to 03-2024 (left column, no valid data in the final campaign dataset), 03-2024 to 07-2024 (middle column) and 07-2023 to 07-2024 (right column)..... 41

Figure 6-13 Current speed Hovmöller diagrams of the calibrated model results and the observations from HS-1-CP. The plot in the top row is with the observations considered in Deltares (2024), the plot in the bottom row is with the final campaign observations and the plot in the bottom row is with the model results..... 42

Figure 6-14 Current magnitude 3D profile plots comparisons between the calibrated 3D model results (dashed lines) and the observations (full lines) from HS-1-CP. The plot in the top row is for the observations considered in Deltares (2024), the plots in the bottom row are for the final campaign observations. The periods covered by the data are 07-2023 to 03-2024 (left column), 03-2024 to 07-2024 (middle column) and 07-2023 to 07-2024 (right column)..... 43

Figure 7-1 Hovmöller diagrams of the 3D temperature model results (background colour map) and near-bottom and near-surface temperature observations (coloured circles) from KG-1-CP and KG-1-LB, respectively. The vertical line indicates the date until which the observation data have been considered in the Deltares (2024). 44

Figure 7-2 Hovmöller diagrams of the 3D temperature model results (background colour map) and near-bottom and near-surface temperature observations (coloured circles) from HS-1-CP and HS-1-LB, respectively. The vertical line indicates the date until which the observation data have been considered in the Deltares (2024). 44

Figure 8-1 Timeseries comparisons between the calibrated model results and the observations from KG-1-LB of significant wave height (top panel), peak wave period (middle panel) and mean wave direction (bottom panel). The vertical line indicates the date until which the observation data have been considered in the Deltares (2024). 46

Figure 8-2 Density scatter comparisons between the calibrated model results and the observations from KG-1-LB of significant wave height (top row), peak wave period (middle row) and mean wave direction (bottom row). The periods covered by the data are 07-2023 to 12-2023 (left column), 01-2024 to 07-2024 (middle column) and 07-2023 to 07-2024 (right column). 47

Figure 8-3 Timeseries comparisons between the calibrated model results and the observations from HS-1-LB of significant wave height (top panel), peak wave period (middle panel) and mean wave direction (bottom panel). The vertical line indicates the date until which the observation data have been considered in the Deltares (2024). 48

Figure 8-4 Density scatter comparisons between the calibrated model results and the observations from HS-1-LB of significant wave height (top row), peak wave period (middle row) and mean wave direction (bottom row). The periods covered by the data are 07-2023 to 12-2023 (left column), 01-2024 to 07-2024 (middle column) and 07-2023 to 07-2024 (right column). 49

List of Tables

Table 3-1 Coordinates of the Kattegat en Hesselø South stations. 13
Table 3-2 Considered Kattegat observation data. 14
Table 3-3 Considered Hesselø South observation data..... 15

Nomenclature

Variable	Abbreviation	Unit
Atmosphere		
Wind speed @ 10 mMSL height	U_{10mag}	m/s
Wind direction @ 10 mMSL height	U_{10dir}	°N (clockwise from)
Wind speed @ 150 mMSL height	U_{150mag}	m/s
Wind direction @ 150 mMSL height	U_{150dir}	°N (clockwise from)
Ocean		
Water level	WL or SWL	mMSL
Current speed	CS CSxyy (x: level or s=near-surface, b=near-bottom, m=mid-depth or a=depth-averaged, yy: tot, tid, res) or u_{dir} or $u_{yy,xx}$ (yy: total, tide, res, xx: level or DA)	m/s
Current direction	CD CDxyy (xx: level or s=near-surface, b=near-bottom, m=mid-depth or a=depth-averaged, yy: tot, tid, res) or u_{dir} or $u_{dir,yy,xx}$ (yy: total, tide, res, xx: level or DA)	°N (clockwise to)
Sea surface temperature	SST	°C
Water temperature @ {x} m depth	$T_{sw\{x\}}$	°C
Waves		
Significant wave height	H_{m0} or H_s	m
Peak wave period	T_p	s
Mean wave direction	MWD	°N (clockwise from)
Definitions		
Coordinate System	WGS84 EPSG 4326 (unless specified differently)	
Direction	Clockwise from North	
Wind	°N coming from	
Current	°N going to	
Waves	°N coming from	
Time	Times are relative to UTC	
Vertical Datum	MSL (unless specified differently)	

Statistics	
RMSE	root-mean-square error
ρ	correlation coefficient
σ	standard deviation
R	symmetric slope
n	sample size

Abbreviations	
3D	3-dimensional
DMI	Danish Meteorological Institute
DNV	Det Norske Veritas
ECMWF	European Centre for Medium-Range Weather Forecasts
EMODnet	The European Marine Observation and Data Network
ERA5	ECMWF Re-analysis v5
FEED	Front-End Engineering Design
HS	Hesselø South
IEC	International Electrotechnical Commission
ISO	International Organization for Standardization
KG	Kattegat
mMSL	Metres above Mean Sea Level
MSL	Mean Sea Level
OWF	Offshore Wind Farm
UTC	Coordinated Universal Time
WGS84	World Geodetic System 1984

1 Summary

The Danish Energy Agency has tasked Energinet (the Client) with undertaking site metocean conditions assessments for the development of the offshore wind farm areas Kattegat and Hesselø South. So far, the study involved the metocean data basis report and database (Part A) and the metocean data analysis reports (parts B and C).

This note presents the reverification of the metocean hindcast data used as input in the assessments of the metocean site conditions. More precisely, in this reverification note, measurements from the metocean measurement campaigns carried out in the offshore wind farm areas Kattegat and Hesselø South and, which were still not available at the time the metocean study was carried out, are compared to metocean hindcast data produced and calibrated in the same way as the data in the metocean database (Part A report, Deltares, 2024). The parameters considered in this reverification note are wind speed and direction, wave height, period and direction, current speed, still water level and water temperature. The conclusion is that the reverification of all the parameters mentioned does not change any of the conclusions made in the Part A report. The quality of the basis data is as reported and there is no need for recalibration.

2 Introduction

2.1 Background

The Danish Energy Agency has tasked Energinet (the Client) with undertaking site metocean conditions assessments for the development of the offshore wind farm areas Kattegat (KG) and Hesselø South (HS). The offshore wind farms are to be in Kattegat east of the Danish peninsula Djursland. An overview is shown on Figure 2-1.

The site metocean conditions assessments, which are to be certified, will form part of the larger site conditions assessment work (also including site wind and ice conditions assessments) and will be a part of the technical basis for the future public tender on the development of offshore wind farms within the areas. The site metocean conditions assessment must be suitable for the Front-End Engineering and Design (FEED) of offshore wind turbine generators and other support structures for the offshore wind farms.



Figure 2-1 Overview map of the windfarm areas Kattegat and Hesselø. The dashed line indicates the full data delivery area, and the full line indicate the OWFs.

The full study consists of several deliverables:

- Part A: Description and Verification of Data Basis (Deltares, 2024).
- Part B: Data Analyses and Results (report for Kattegat, Sweco, 2024a).
- Part C: Data Analyses and Results (report for Hesselø South, Sweco, 2024b).
- Long-term hindcast data (digital timeseries, delivered with Part A, Deltares, 2024).
- Measurement data (digital timeseries, Fugro, 2024a,b).
- Part D: Reverification of Data Basis (this report).

All deliverables except for Part D, this report, are already completed.

2.2 Objectives

In Part A of the study metocean data, which serves as input for the assessment of the MetOcean site conditions to support the design of the various structures within the offshore wind farm areas Kattegat and Hesselø South have been derived. These data, which originate from hourly model results covering a long period, namely from 1979 until 2023, have been validated and calibrated using measurement data available in the area. In particular data from the metocean measurement campaign carried out by Fugro have been used to validate and calibrate the model results. However, at the time of the Part A study the full metocean measurement campaign data were not yet available. The campaigns took place from 21-07-2023 to 21-07-2024 and in the Part A study data until up to April 2024 have been considered.

The measurement campaigns are now ended and Fugro (2024a,b) has quality controlled the whole campaigned data and released the final metocean campaign datasets. The purpose of this note is to reverify metocean hindcast data produced and calibrated in the same way as the data in the metocean database (Part A report, Deltares, 2024) using measurements from the metocean measurement campaigns carried out in the offshore wind farm areas Kattegat and Hesselø South and which were not considered in Deltares (2024).

2.3 Approach

The computations of Deltares (2024) have been extended until the end of July 2024 using the same models and applying the same calibration factors as in the derivation of deliverable “Long-term hindcast data” (digital timeseries, delivered with Part A report, Deltares, 2024). These data are compared with the full campaign data for the period considered in Deltares (2024), the period for which data are now available and which had not been considered in Deltares (2024) and the full campaign data. The aim of the comparisons is to identify whether the quality of the model results considering the extra measurement data is comparable to the quality assessed in the data basis study (Deltares, 2024). The variables being considered are wind speed, water level, current speed, significant wave height, peak wave period and mean wave direction. The comparisons are made qualitatively by means of timeseries and Hovmöller plots and quantitatively by means of density scatter plots, quantile-quantile comparisons and errors statistics. In addition, for currents, the vertical current speed profiles are also compared.

Because the water level and current data can contain inhomogeneities due to variations in the location of the sensors, deterioration of the current speed signal due to interferences or contaminations, the final quality assured dataset can differ significantly from the monthly datasets delivered during the campaign. Because of this, in the comparisons between the water level and current model results with the observations we also plot the observation data considered in Deltares (2024). The difference between the monthly and the final wave and wind data are generally not significant and, therefore, in the reverification of the wind and wave data we only consider the final campaign data.

3 Overview of measurement campaign data

3.1 Introduction

The Kattegat and Hesselø South measurement campaigns are described in Fugro (2024a) and Fugro (2024b), respectively. The locations where the instruments have been deployed are shown in Figure 3-1 and the coordinates are given in Table 3-1. A short description of the campaigns is given in Section 3.2 for the Kattegat (KG-1) data and in Section 3.3 for the Hesselø South (HS-1) data.

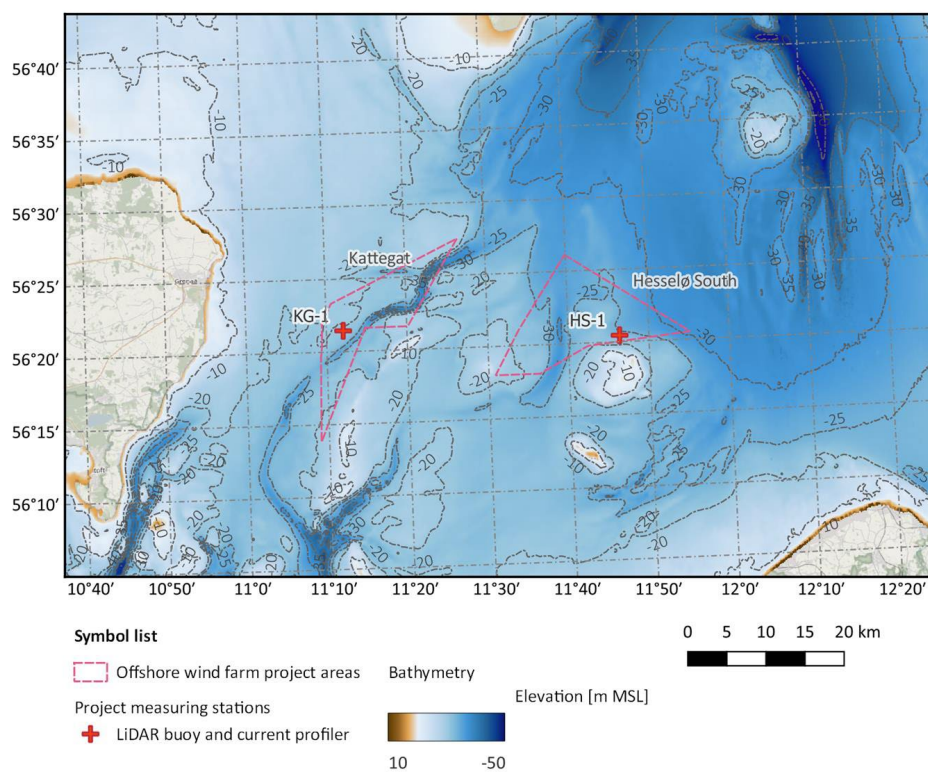


Figure 3-1 Instrument locations in the Kattegat and Hesselø project area. Figure taken from Fugro (2024a).

Table 3-1 Coordinates of the Kattegat en Hesselø South stations.

Station	Longitude (°E)	Latitude (°N)	Depth (mMSL)
KG-1-LP	11.2010	56.3506	20.8
KG-1-CP	11.2011	56.3503	20.7
HS-1-LP	11.7723	56.3340	22.6
HS-1-CP	11.7722	56.3342	22.6

3.2 Kattegat measurement campaign

The Kattegat measurement campaign is described in Fugro (2024a). The wind LiDAR buoy WS199 (21-07-2023 to 21-07-2024) was deployed at Kattegat together with a bottom mounted water level sensor, station KG-1-LB, and a bottom mounted upward-looking current profiler, station KG-1-CP. The instruments in the buoy include the wind LiDAR, the wave sensor and the downward-looking current profiler. During the campaign period two upward-looking current profilers have been deployed:

- 104507 from 21-07-2023 to 22-02-2024 (D1) and
- 104510 from 22-02-2024 to 21-07-2024 (D2).

The KG-1-LB current data are available with 1 m intervals from -3 to -17 mMSL. The KG-1-CP current data are available with 1 m intervals from 4 to 18 m from bottom from 21-07-2023 until 22-02-2024 (D1) and also from 4 to 18 m from bottom from 22-02-2024 until 21-07-2024 (D2). Table 3-2 provides an overview of the instruments and considered variables.

Table 3-2 Considered Kattegat observation data.

Station	Sensor	Variable	Period
KG-1-LB	Wind: ZephIR ZX300M CW LiDAR	12 mMSL and 150 mMSL wind speed and direction	07-2023 – 07-2024
KG-1-LB	WL (bottom pressure): Thelma Biotel TBR700	Water pressure and water level	07-2023 – 07-2024
KG-1-LB	Current: Nortek Aquadopp 400 kHz	Current speed at 1 m intervals from -3 to -17 mMSL	07-2023 – 07-2024
KG-1-LB	Waves: Wavesense 3	H _s , T _p , MWD	07-2023 – 07-2024
KG-1-CP	WL (Bottom pressure) and Current: Nortek Signature 500	Water pressure, water level and current speed at 1 m intervals at 4 to 18 m from bottom	07-2023 – 02-2024 (D1) and 02-2024 – 07-2024 (D2)

3.3 Hesselø South measurement campaign

The Hesselø South measurement campaign is described in Fugro (2024b). The wind LiDAR buoy SWLB059 was deployed at Hesselø South on 21 July 2023 together with a bottom mounted water level sensor, station HS-1-LB, and a bottom mounted upward-looking current profiler (104503), station HS-1-CP. The instruments in the buoy include the wind LiDAR, the wave sensor and the downward-looking current profiler. On 23 March 2024, buoy SWLB059 (21-07-2023 to 23-03-2024) was replaced with buoy WS190 (23-03-2024 to 21-07-2024) and profiler 104503 (21-07-2023 to 23-03-2024) replaced with profiler 104507 (23-03-2024 to 21-07-2024).

Unfortunately, the seabed water pressure sensor (Thelma) at HS-1-LB stopped working after 5 days from the initial deployment. The HS-1-LB current data are available with 1 m intervals from -3 to -19 mMSL. The HS-1-CP current data are available with 1 m intervals from 5 to 21 m from bottom from 21-07-2023 until 22-03-2024 (D1) and from 4 to 20 m from bottom from 23-03-2024 until 21-07-2024 (D2). Table 3-3 provides an overview of the instruments and considered variables.

Table 3-3 Considered Hesselø South observation data.

Station	Sensor	Variable	Period
HS-1-LB	Wind: ZephIR ZX300M CW LiDAR	12 mMSL and 150 mMSL wind speed and direction	07-2023 – 07-2024
HS-1-LB	WL (bottom pressure): Thelma Biotel TBR700	Water pressure and water level	07-2023 – 07-2024
HS-1-LB	Current: Nortek Aquadopp 400 kHz	Current speed at 1 m intervals from -3 to -19 mMSL	07-2023 – 07-2024
HS-1-LB	Waves: Wavesense 3	H_s , T_p , MWD	07-2023 – 07-2024
HS-1-CP	WL (Bottom pressure) and Current: Nortek Signature 500	Water pressure, water level and current speed at 1 m intervals at 5 to 21 m from bottom	07-2023 – 03-2024
HS-1-CP	WL (Bottom pressure) and Current: Nortek Signature 500	Water pressure, water level and current speed at 1 m intervals at 4 to 20 m from bottom	03-2023 – 07-2024

4 Wind reverification

4.1 Introduction

The following sections 4.2 and 4.3 show the comparisons between the calibrated model results and the observations of wind from KS-1 and HS-1, respectively. The considered variables are the 10 mMSL and the 150 mMSL (hub height) wind speeds and directions.

4.2 Kattegat wind

Figure 4-1 shows the timeseries comparisons between the model data of wind speed and direction at 10 mMSL and the observations 12 mMSL observations of wind speed and direction converted to 10 mMSL at KG-1-LB. In this and other timeseries figures in this report, the red vertical line indicates the period until which the observation data have been considered in the validation of the model results for the variable in question in Deltares (2024).

Figure 4-2 shows the density scatter comparisons between the calibrated model results and the observations of wind speed and direction at 10 m for three periods:

1. the period considered in Deltares (2024), i.e. the period until the red line in Figure 4-1,
2. the extra campaign data period, of which the observations were not considered in Deltares (2024), i.e. the period after the red line in Figure 4-1, and
3. the whole campaign period

In the density scatter comparison plots in Figure 4-2 and other in this report, the colours indicate the data density, with darker colours indicating higher data density. The plots include main statistics of the data comparisons such as the correlation coefficient, root-mean-square errors, bias and standard deviation between the dataset. Appendix A describes of how these statistics were computed. The presented statistics depend on whether linear (speeds, heights and periods), as in the top panels of Figure 4-2, or circular (directions) variables, as in the bottom panels of Figure 4-2 are plotted. Furthermore, in the plots of linear variables, the plots also include percentile comparisons and two fits are given: a symmetric fit (red dotted line) to the whole data (plotted in terms of density) and a linear fit (dashed blue line) through the data percentiles (the blue pluses, with each one corresponding to one percentile pair, 101 pluses in total, indicating the 1.00th to the 99.00th with increases of 1 and the 99.90th and the 99.99th). The red line provides an indication of the relation between the bulk of the data. The symmetric slop is given as it provides a direct measure of the (percentage of) over- or underestimation. The blue line provides an indication of the linear relation between the data extremes, with the considered percentiles being the plotted 1st to the 99.99th.

Figure 4-1 shows that the wind speeds in the period of the KG-1-LB campaign which is not considered in Deltares (2024), is milder than the period before (cf. the period before and after the red line in Figure 4-1). Nevertheless, Figure 4-1 and Figure 4-2 show that the correspondence between the model results and the KG-1-LB observations is similar in the considered periods with comparable coefficients, in spite of the correlations being as expected slightly lower in the milder period (March-July).

Figure 4-3 shows the timeseries comparisons between the model results and the observations of the 150 mMSL wind speeds and directions at KG-1-LB. The respective density scatter comparisons are given in Figure 4-4. The figures show also that the correspondence between the model results and the KG-1-LB observations of the 150 mMSL wind speeds and directions is also similar in the considered periods, with comparable correlation and fit coefficients, in spite of slightly lower correlations in the milder period.

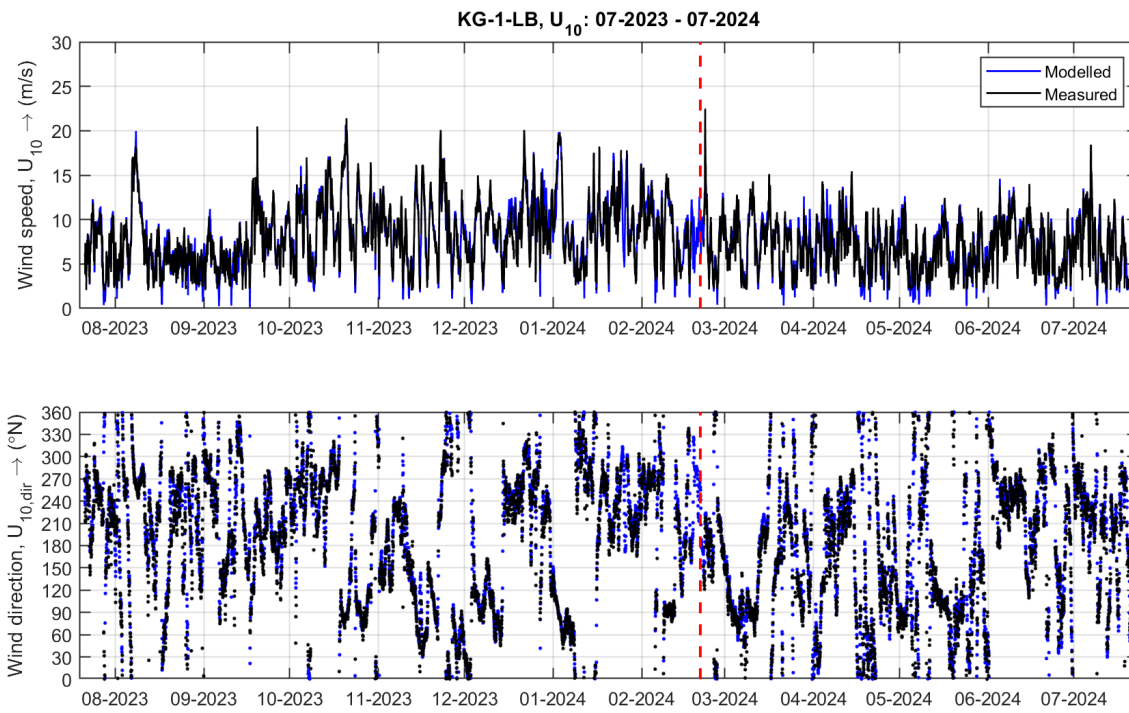


Figure 4-1 Timeseries comparisons between the calibrated model results and the observations from KG-1-LB of 10 m wind speed (top panel) and direction (bottom panel). The vertical line indicates the date until which the observation data have been considered in the Deltares (2024).

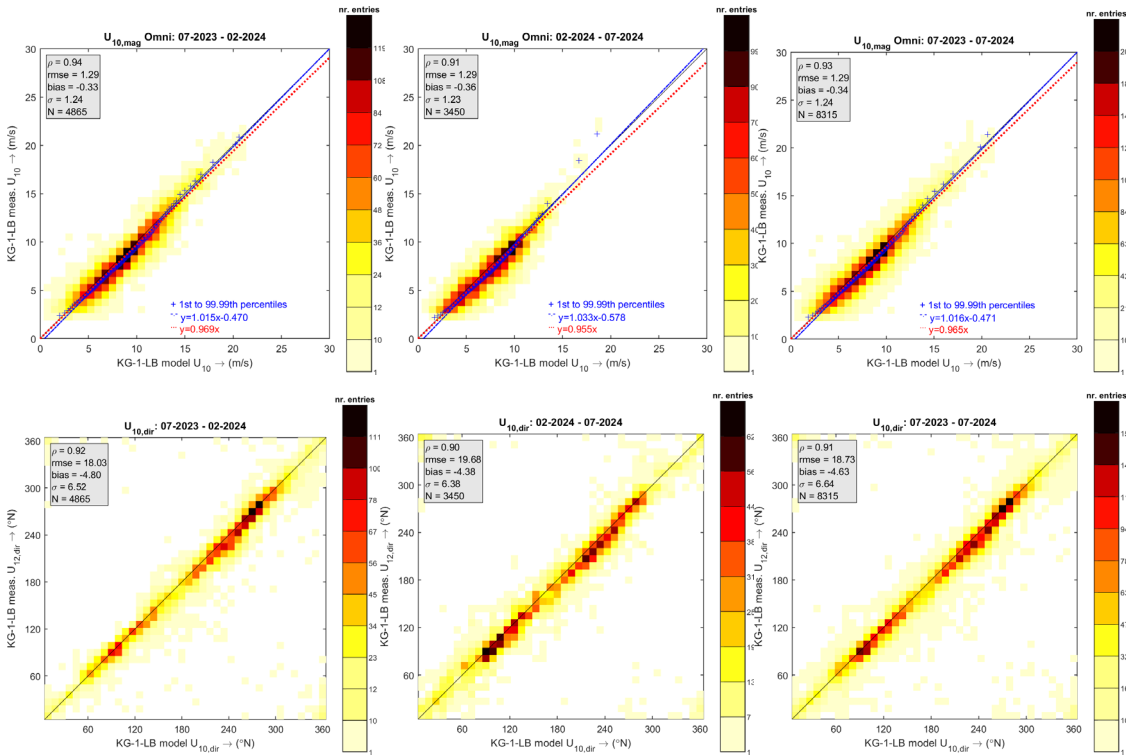


Figure 4-2 Density scatter comparisons between the calibrated model results and the observations from KG-1-LB of 10 m wind speed (top row) and direction (bottom row). The KG-1-LB wind speed observations at 12 mMSL were converted to 10 mMSL. The periods covered by the data are 07-2023 to 02-2024 (left column), 02-2024 to 07-2024 (middle column) and 07-2023 to 07-2024 (right column).

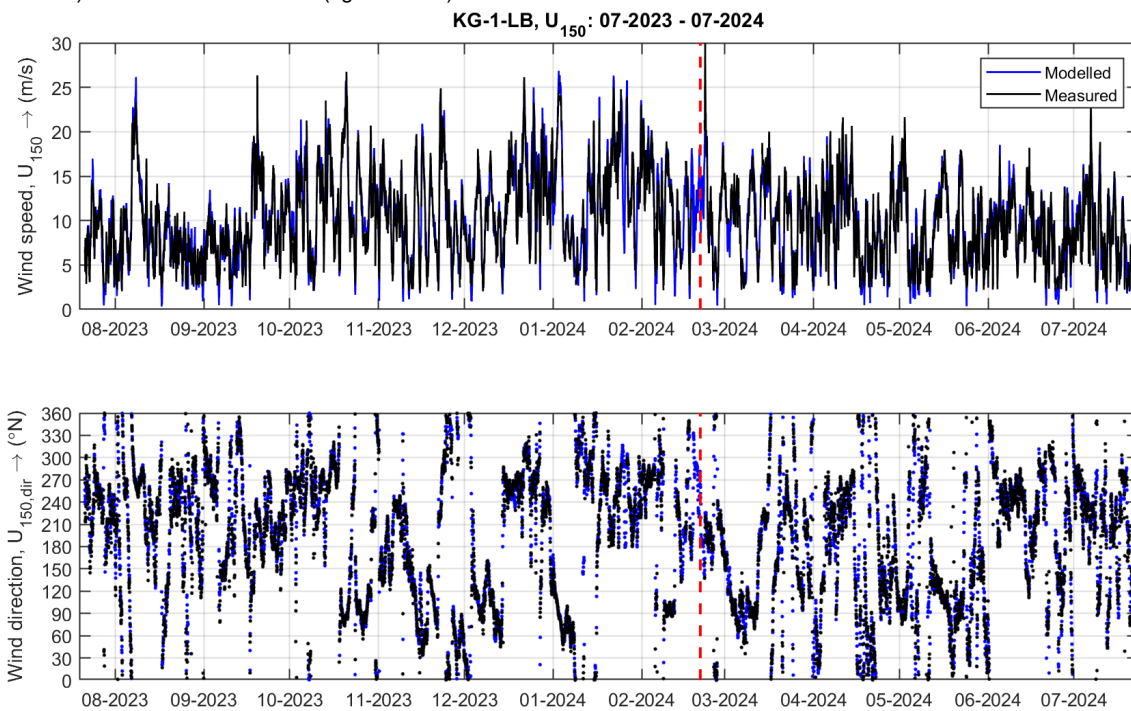


Figure 4-3 Timeseries comparisons between the calibrated model results and the observations from KG-1-LB of 150 mMSL wind speed (top panel) and direction (bottom panel). The vertical line indicates the date until which the observation data have been considered in the Deltares (2024).

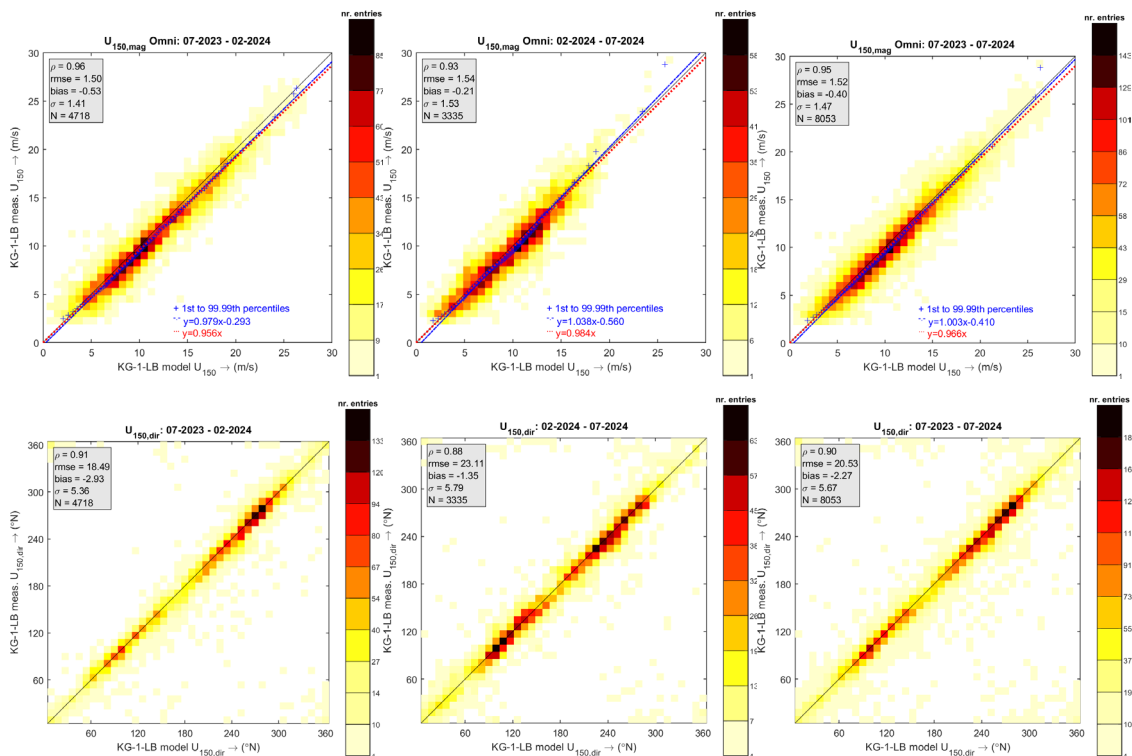


Figure 4-4 Density scatter comparisons between the calibrated model results and the observations from KG-1-LB of 150 mMSL wind speed (top row) and direction (bottom row). The periods covered by the data are 07-2023 to 02-2024 (left column), 02-2024 to 07-2024 (middle column) and 07-2023 to 07-2024 (right column).

4.3 Hesselø South wind

Figure 4-5 shows the timeseries comparisons between the model data of wind speed and direction at 10 mMSL and the LiDAR observations of wind speed and direction at 12 mMSL converted to 10 mMSL at KG-1-LB. Figure 4-6 shows the respective density scatter comparisons in the considered three periods. Figure 4-7 shows the timeseries comparisons between the model results and the observations of the 150 mMSL wind speeds and directions at KG-1-LB. The respective density scatter comparisons are given in Figure 4-8.

The timeseries figures show again that the data from the period not considered in Deltares (2024) are milder, leading to as expected a slightly lower correlation between the modelled and observed wind speeds, but the correspondence between the model results and the observations for the different time periods is still high and comparable. The density scatter plots also show that the error statistics are also very similar in the considered three periods of data.

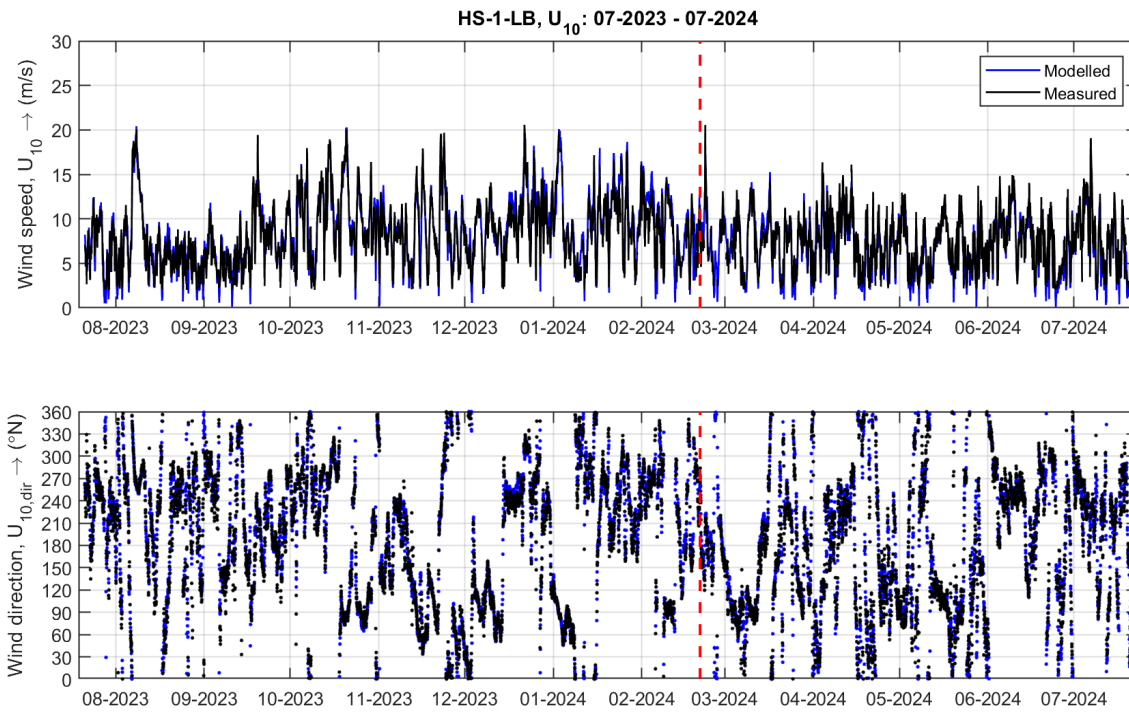


Figure 4-5 Timeseries comparisons between the calibrated model results and the observations from HS-1-LB of 10 m wind speed (top panel) and direction (bottom panel). The vertical line indicates the date until which the observation data have been considered in the Deltares (2024).

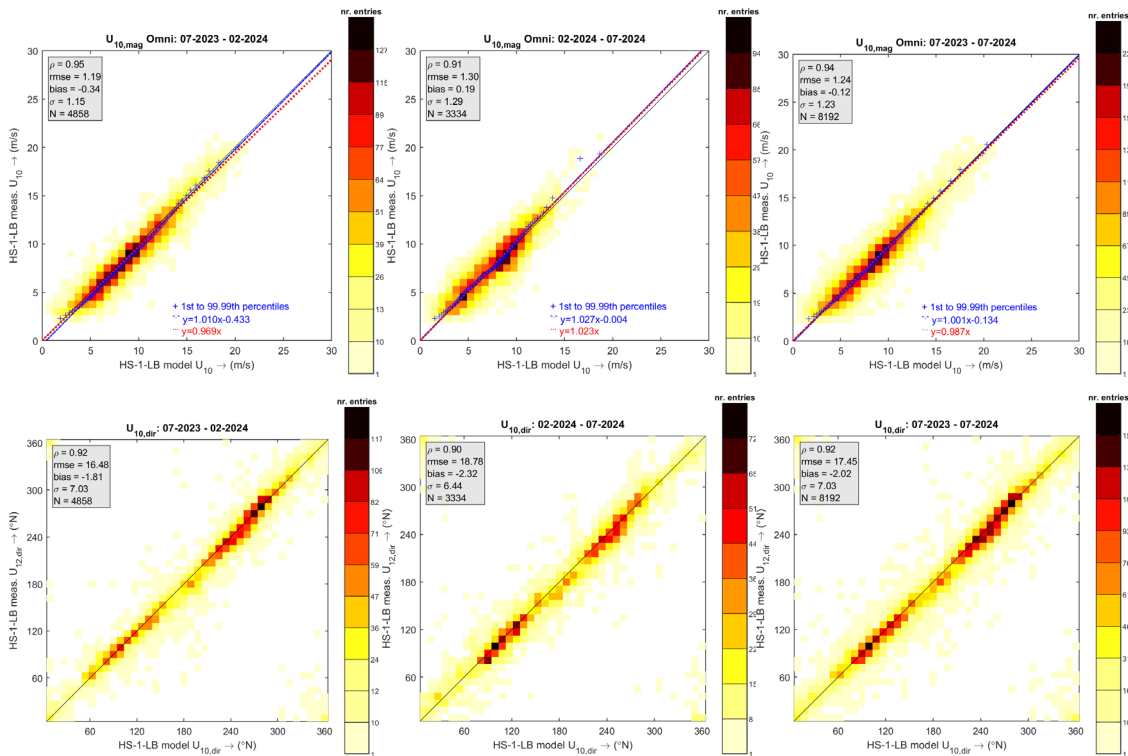


Figure 4-6 Density scatter comparisons between the calibrated model results and the observations from HS-1-LB of 10 m wind speed (top row) and direction (bottom row). The HS-1-LB wind speed observations at 12 mMSL were converted to 10 mMSL. The periods covered by the data are 07-2023 to 02-2024 (left column), 02-2024 to 07-2024 (middle column) and 07-2023 to 07-2024 (right column).

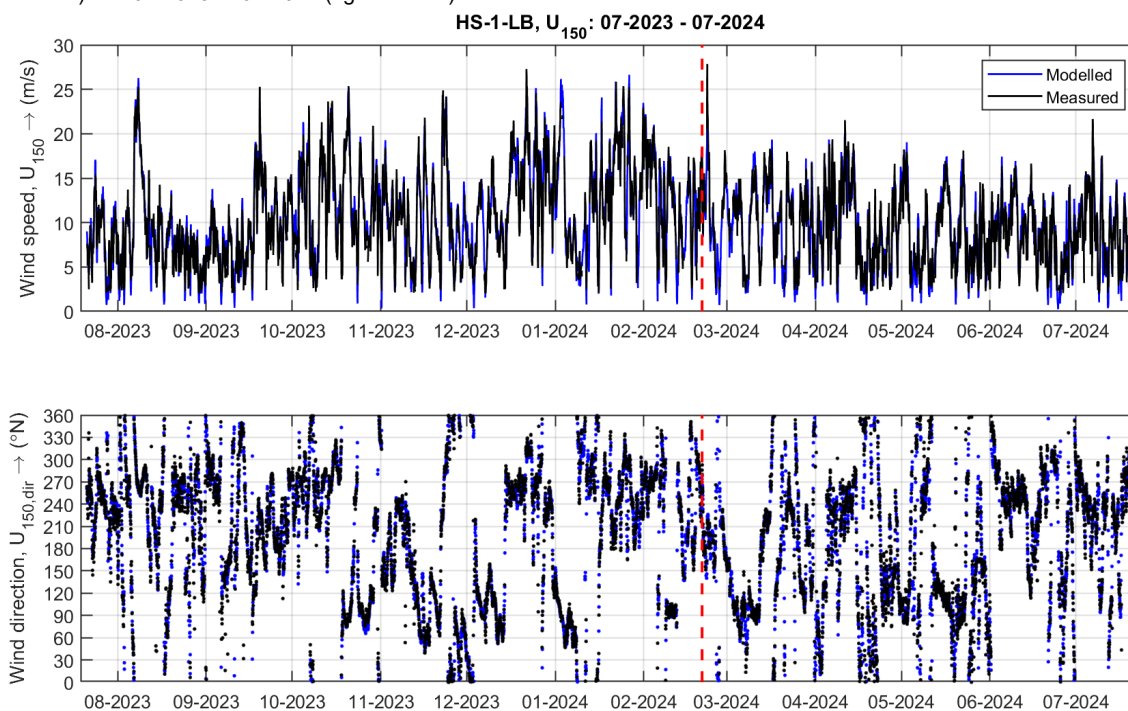


Figure 4-7 Timeseries comparisons between the calibrated model results and the observations from HS-1-LB of 150 mMSL wind speed (top panel) and direction (bottom panel). The vertical line indicates the date until which the observation data have been considered in the Deltares (2024).

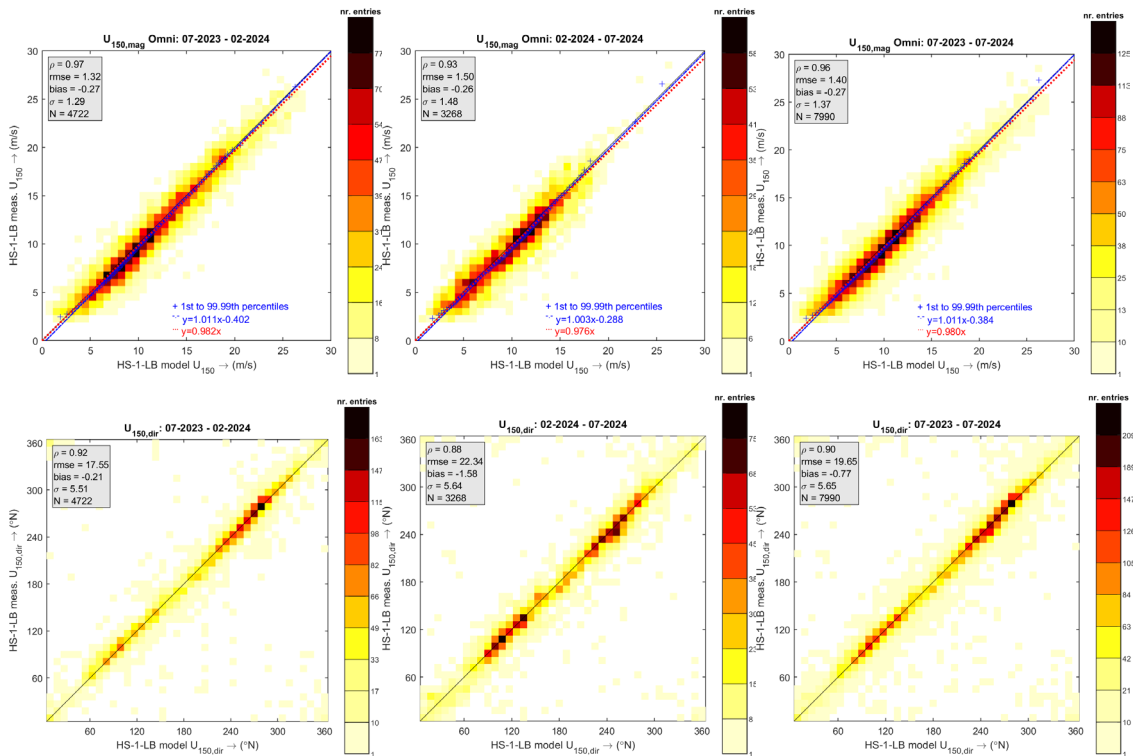


Figure 4-8 Density scatter comparisons between the calibrated model results and the observations from HS-1-LB of 150 mMSL wind speed (top row) and direction (bottom row). The periods covered by the data are 07-2023 to 02-2024 (left column), 02-2024 to 07-2024 (middle column) and 07-2023 to 07-2024 (right column).

5 Water level reverification

5.1 Introduction

The following sections 5.2 and 5.3 show the comparisons between the calibrated model results and the water level observations from KS-1 and HS-1, respectively.

The bottom-mounted instruments used in the Fugro campaigns measure the water pressure, which can be used to compute the total or still water level (SWL). In the files provided by Fugro (2024a,b) with final campaign offline data, the water levels are directly available. In the data basis study only the water pressure observations were available and we have converted these into water levels. Furthermore, given that water level observations are by nature inhomogeneous, with variations in the location of the sensor generally leading to jumps in the observed levels, in the density scatter comparisons shown the monthly bias between the model and the observations has been removed. Also due to the inhomogeneous nature of the water level observations, the final quality assured dataset can differ significantly from the monthly datasets delivered during the campaign. Because of this, in the comparisons we also plot the observation data considered in Deltares (2024).

5.2 Kattegat water level

Figure 5-1 shows the timeseries comparisons between the total water level model results and observations from KG-1-LB and KG-1-CP. The respective density scatter comparisons are given in Figure 5-2 (KG-1-LB) and Figure 5-3 (KG-1-CP). As noted, because the final campaign data can significantly differ from the monthly data considered in Deltares (2024), the timeseries plots also include the data considered in Deltares (2024), the grey lines in the figures, and the density scatter plots between the model results and the data considered in Deltares (2024) are also given in the top row of the density scatter figures. As can be seen in Figure 5-1 there are some issues in the KG-1-LB observations considered in Deltares (2024) from 1 December 2023 onwards (cf. grey line in top panel of Figure 5-1) and therefore these data have not been considered in the validation and calibration of the model results (Deltares, 2024). The final campaign water levels still contain inhomogeneities in the KG-1-LB water level data from that period, but the data quality is higher. According, Figure 5-2 shows mismatches between the calibrated model results and the observations. On the other hand, the correspondence between the SWL model results and the observations from KG-1-CP, testifying to the quality of both the model results and the observations. Furthermore, Figure 5-3 shows that the quality of model results is comparable in the period considered in Deltares (2024) and the remaining campaign period.

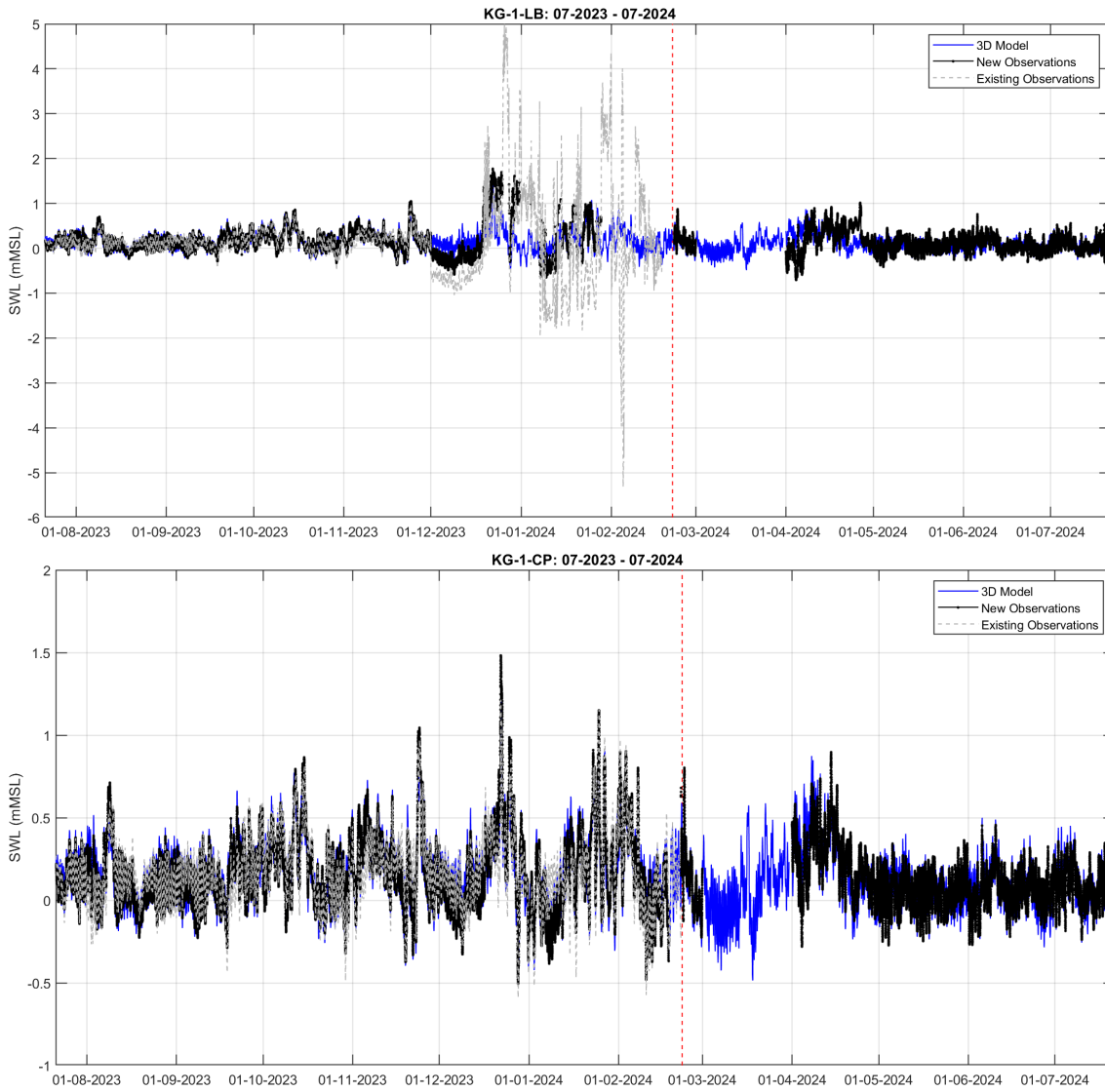


Figure 5-1 Timeseries comparisons between the calibrated model results and the observations from KG-1-LB (top) and KG-1-CP (bottom) of total water level.

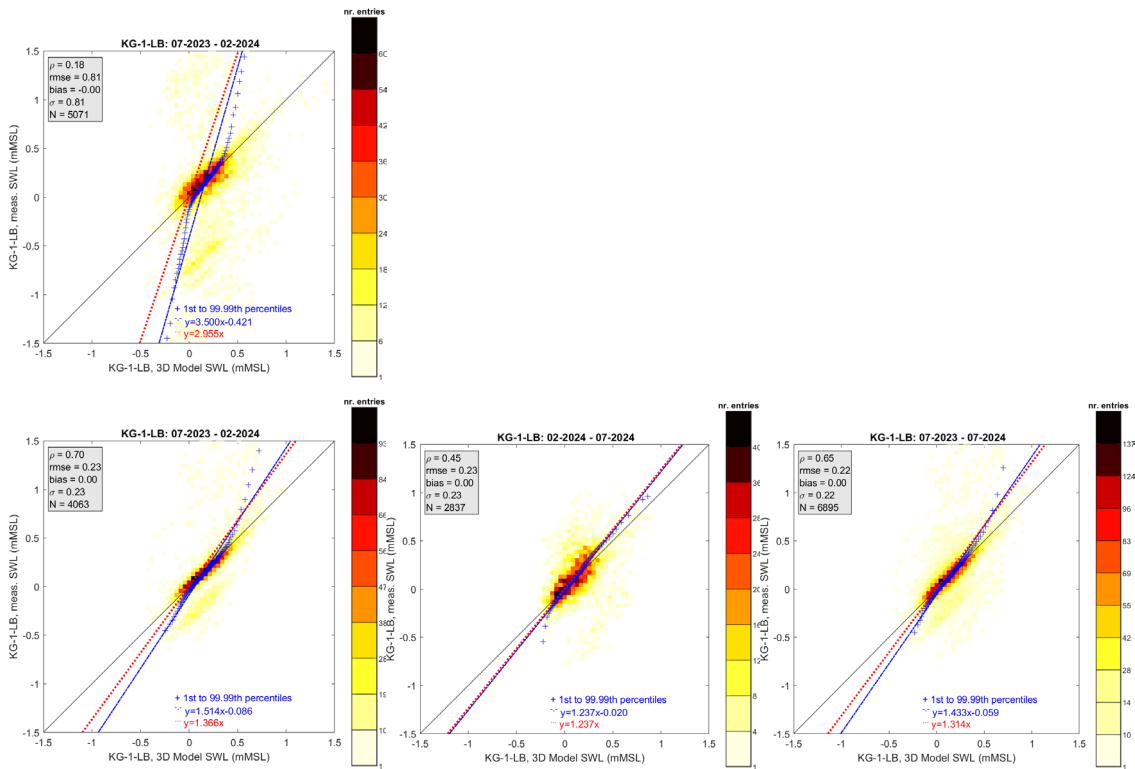


Figure 5-2 Density scatter comparisons between the calibrated 3D model results and the observations from KG-1-LB water level. The plot in the top row is for the observations received during the study, the plots in the bottom row are for the final campaign observations. The periods covered by the data are 07-2023 to 02-2024 (left column), 02-2024 to 07-2024 (middle column) and 07-2023 to 07-2024 (right column).

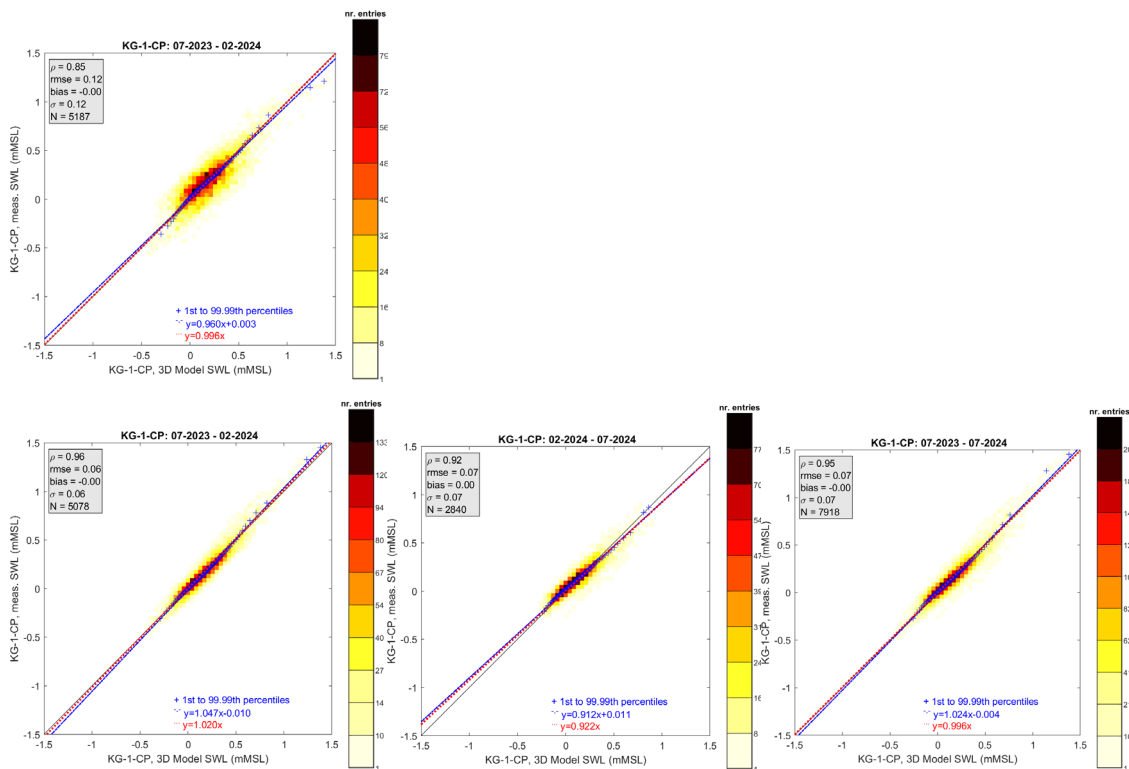


Figure 5-3 Density scatter comparisons between the calibrated 3D model results and the observations from KG-1-CP water level. The plot in the top row is for the observations received during the study, the plots in the bottom row are for the final campaign observations. The periods covered by the data are 07-2023 to 02-2024 (left column), 02-2024 to 07-2024 (middle column) and 07-2023 to 07-2024 (right column).

5.3 Hesselø South water level

Figure 5-4 shows the timeseries comparisons between the total water level model results and observations from HS-1-LB and HS-1-CP. As there are no valid data from HS-1-LB before April 2024, which could be considered in Deltares (2024), Figure 5-5 shows the density scatter comparisons between the model results and the observations from HS-1-LB only for the full observation period. Figure 5-6 shows the density scatter comparisons between the model results and the observations from HS-1-LB for the period considered in Deltares (2024), from July 2023 until March 2024, the extra campaign data period (03-2024 to 07-2024) and the whole campaign period (07-2023 to 07-2024). All figures show a high correspondence between the model results and the HS-1 observations and that the quality of model results is equally high in all considered campaign periods.

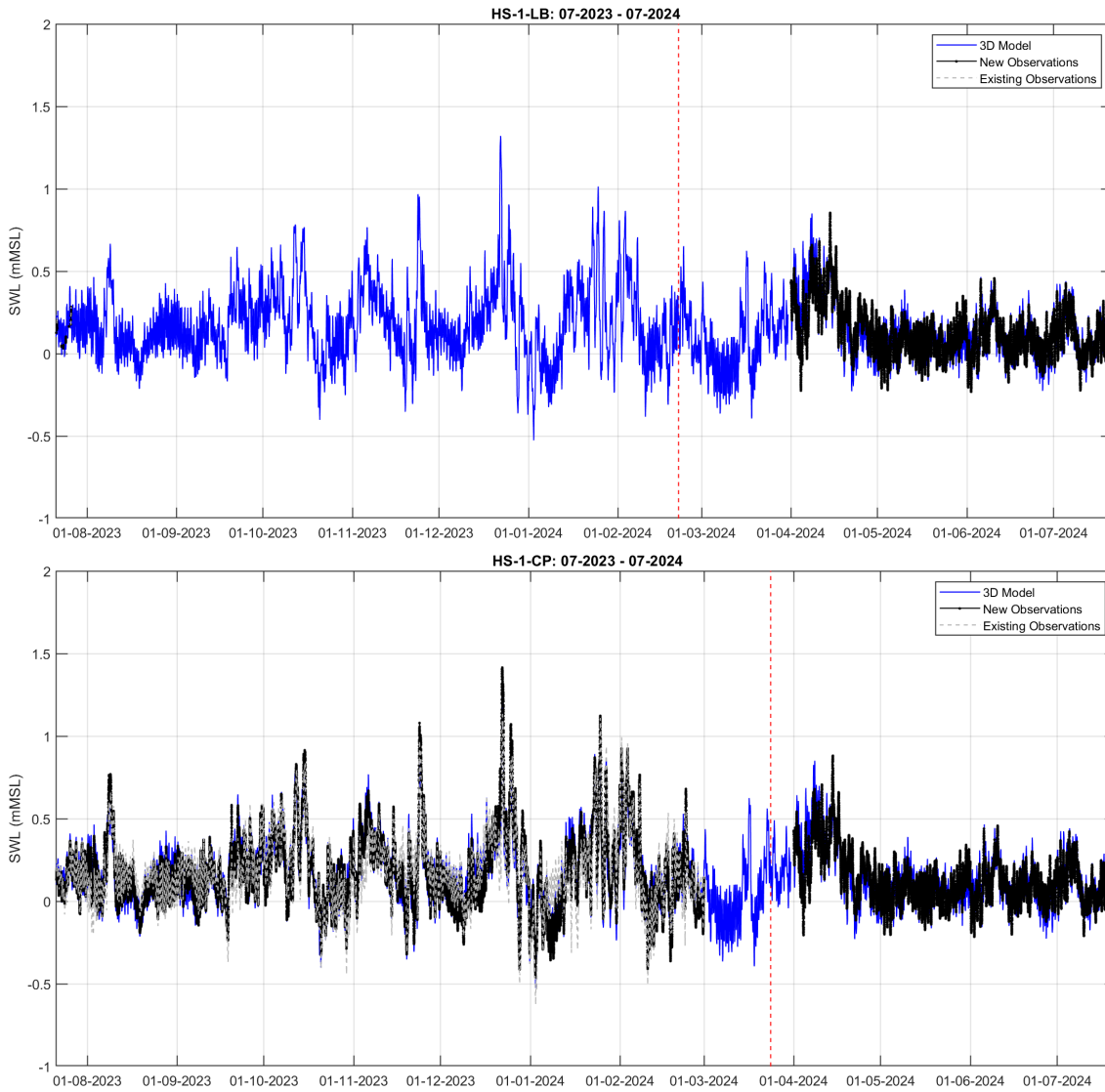


Figure 5-4 Timeseries comparisons between the calibrated model results and the observations from HS-1-LB (top) and HS-1-CP (bottom) of total water level.

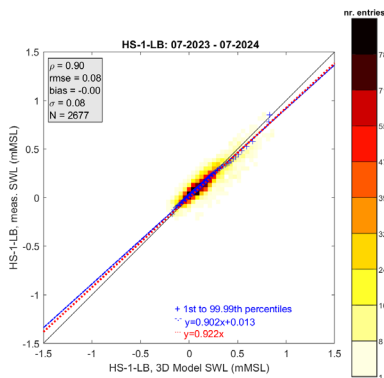


Figure 5-5 Density scatter comparisons between the calibrated 3D model results and the observations from HS-1-LB water level water level from 04-2024 until 07-2024.

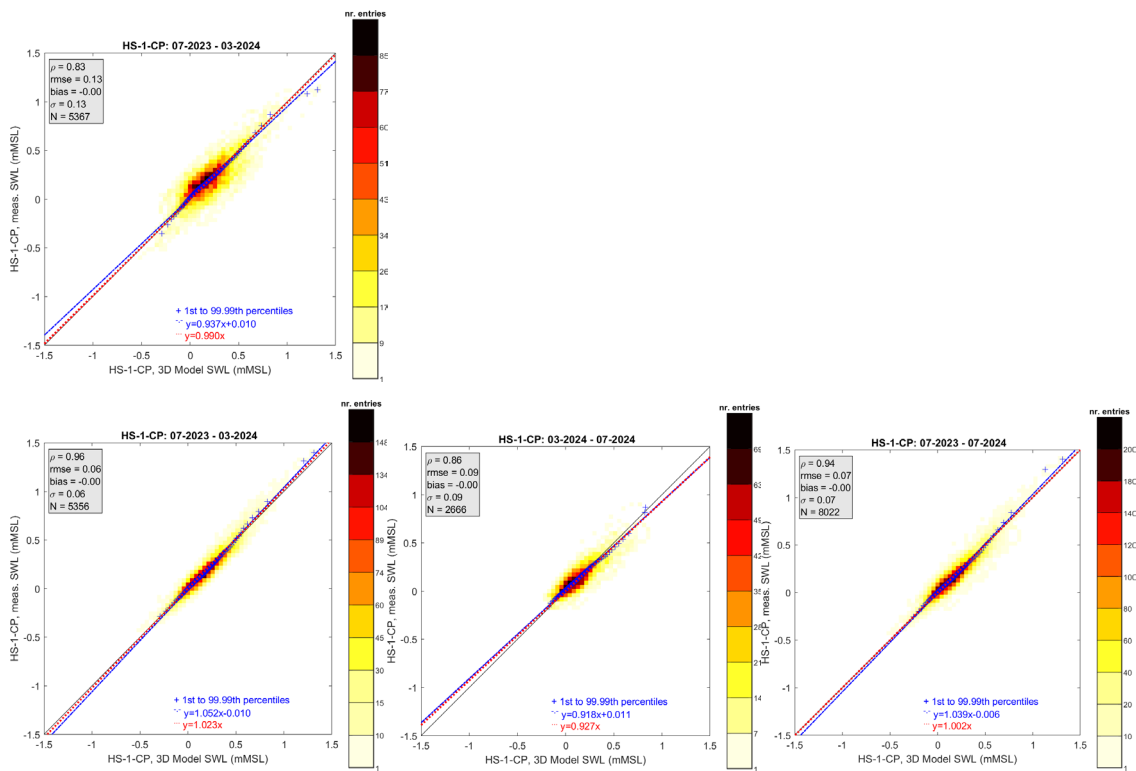


Figure 5-6 Density scatter comparisons between the calibrated 3D model results and the observations from HS-1-CP water level. The plot in the top row is for the observations received during the study, the plots in the bottom row are for the final campaign observations. The periods covered by the data are 07-2023 to 03-2024 (left column), 03-2024 to 07-2024 (middle column) and 07-2023 to 07-2024 (right column).

6 Current reverification

6.1 Introduction

The following sections 6.2 and 6.3 show the comparisons between the calibrated model results and the observations from KS-1 and HS-1, respectively.

The comparisons are made by means of timeseries and density scatters of depth-averaged current speeds, Hovmöller diagrams of the current speed and average vertical current speed profiles. In the depth-averaged comparisons the model results are integrated across the levels of the respective observations.

Because the current speed observations can contain inhomogeneities due to variations in the location of the sensors, deterioration of the current speed signal due to interferences or contaminations, the final quality assured dataset can differ significantly from the monthly datasets delivered during the campaign. Because of this, as in the water level comparisons, we also show the comparisons with the observation data considered in Deltares (2024).

6.2 Kattegat currents

Figure 6-1 shows the timeseries comparisons between the depth-averaged current speed model results and observations from KG-1-LB and KG-1-CP. The respective density scatter comparisons are given in Figure 6-2 (KG-1-LB) and Figure 6-3 (KG-1-CP). For KG-1-LB, although comparable, the figures show a better correspondence between the depth-averaged current speed model results and the observation data considered in Deltares (2024) than the final campaign observation data (cf. top row panel and bottom row right panel of Figure 6-2). The correspondence between the model results and the observations from KG-1-CP is higher than between the model results and the observations from KG-1-LB and again the correspondence between the model results with the observation data from KG-1-CP considered in Deltares (2024) and the full campaign data is comparable (cf. top row panel and bottom row right panel of Figure 6-3).

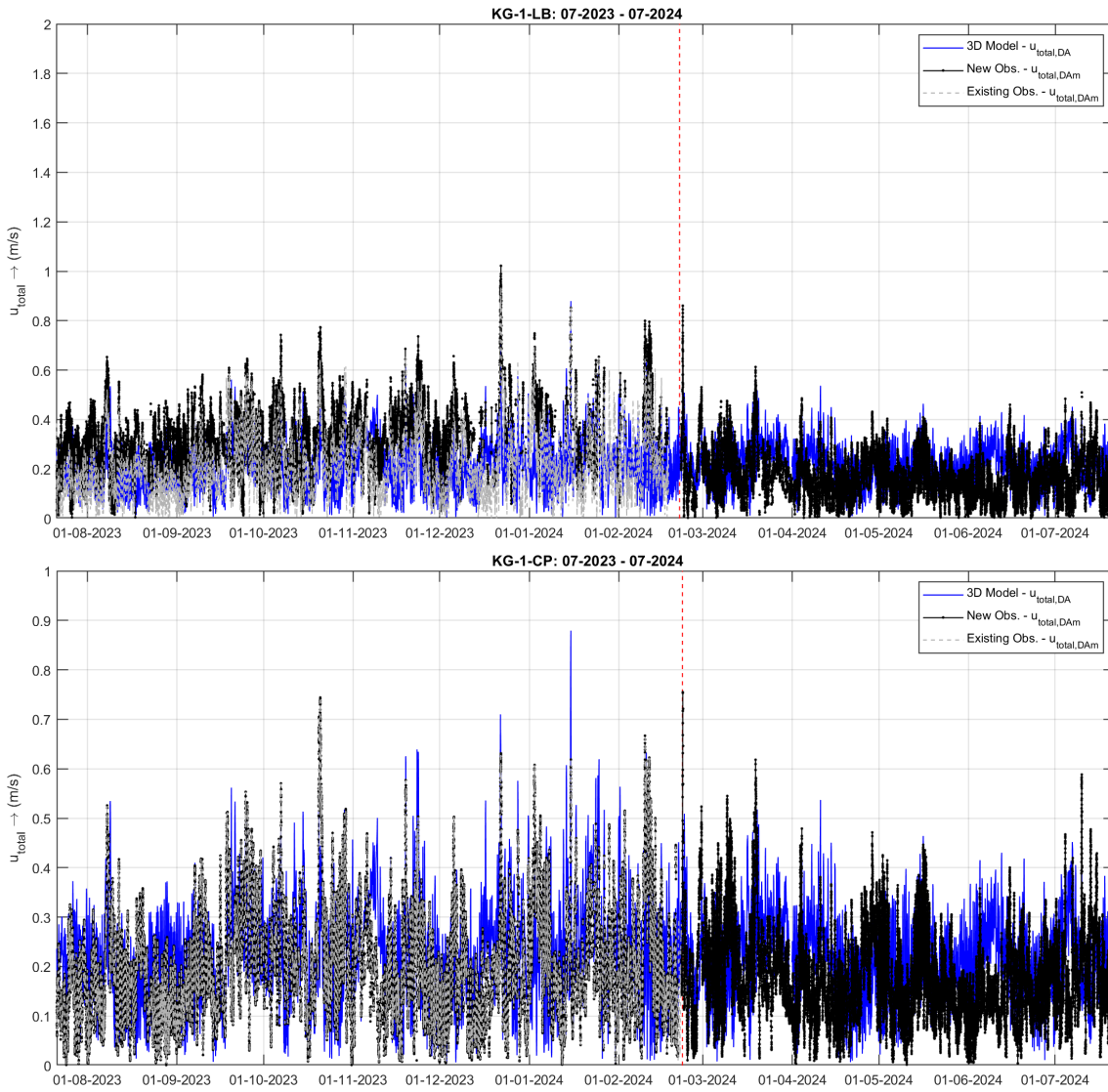


Figure 6-1 Timeseries comparisons between the calibrated model results and the observations from KG-1-LB (top) and KG-1-CP (bottom) of depth-averaged current speed.

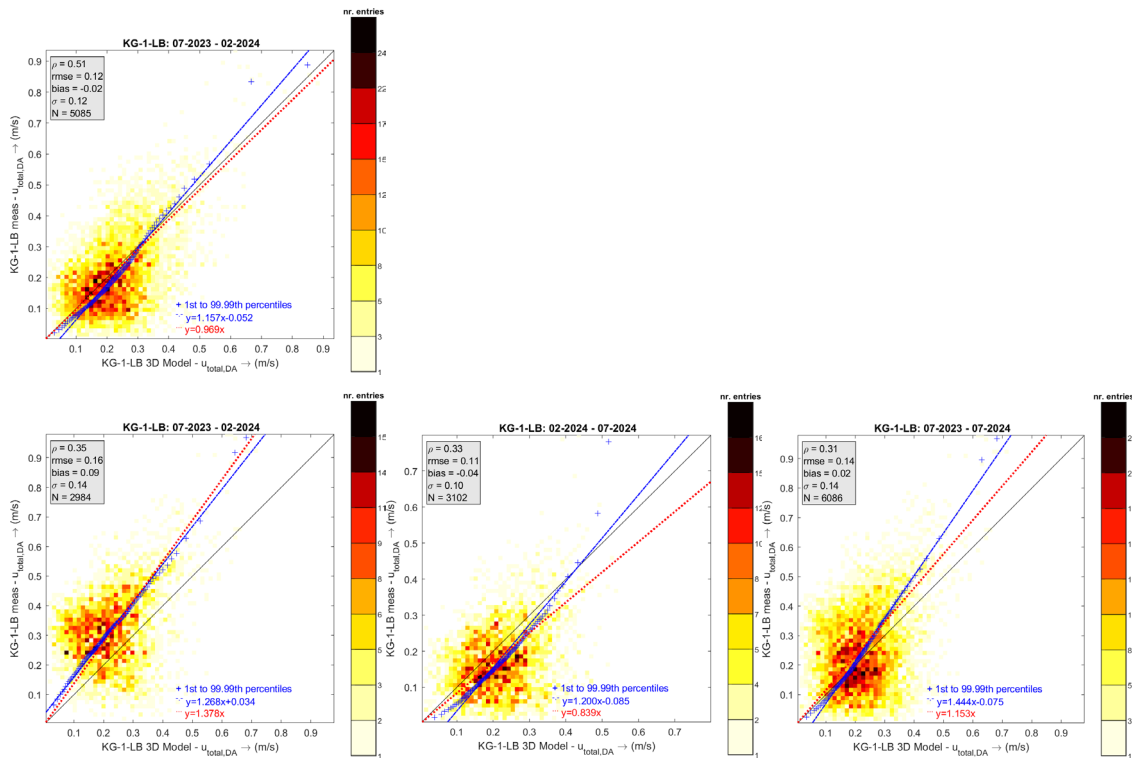


Figure 6-2 Density scatter comparisons between the calibrated 3D model results and the observations from KG-1-LB of depth-averaged current speed. The plot in the top row is for the observations considered in Deltares (2024), the plots in the bottom row are for the final campaign observations. The periods covered by the data are 07-2023 to 02-2024 (left column), 02-2024 to 07-2024 (middle column) and 07-2023 to 07-2024 (right column).

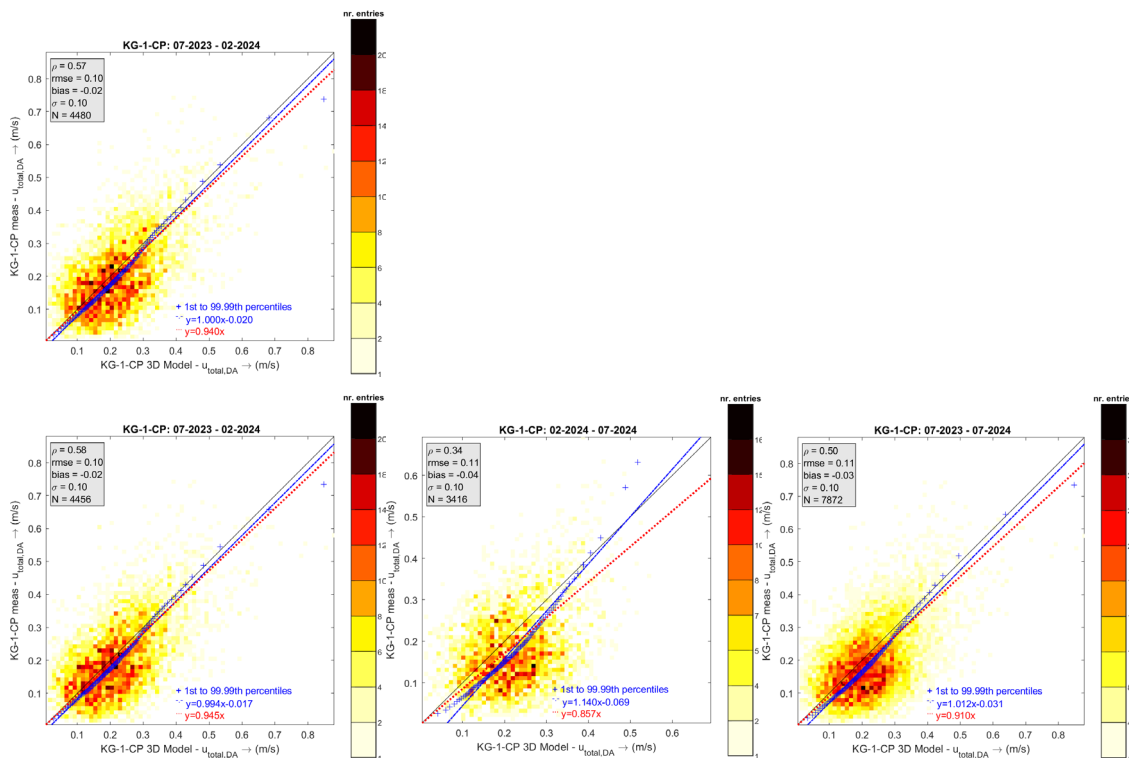


Figure 6-3 Density scatter comparisons between the calibrated 3D model results and the observations from KG-1-CP of depth-averaged current speed. The plot in the top row is for the observations considered in Deltares (2024), the plots in the bottom row are for the final campaign observations. The periods covered by the data are 07-2023 to 02-2024 (left column), 02-2024 to 07-2024 (middle column) and 07-2023 to 07-2024 (right column).

Figure 6-4 shows the Hovmöller diagrams of the KG-1-LB current speed observations considered in Deltares (2024), the final campaign observations and the calibrated 3D model results and Figure 6-5 shows the respective KG-1-LB vertical current speed profile plot comparisons. Figure 6-4 shows that the quality of the KG-1-LB final campaign data from July 2023 until end February 2024 is lower than the data for the same period considered in Deltares (2024) and the final campaign data in the remaining campaign period. Consequently the comparisons between model and observed mean current speed vertical profiles are poorer for the KG-1-LB full campaign data than for the KG-1-LB data considered in Deltares (2024), see Figure 6-5. We consider this lower correspondence to be due to the issues in the observations and not due to a difference in the quality of the model results. Figure 6-6 shows the Hovmöller diagrams of the KG-1-CP current speed observations considered in Deltares (2024), the final campaign observations and the calibrated 3D model results and Figure 6-7 shows the respective KG-1-CP vertical current speed profile plot comparisons. Figure 6-6 and Figure 6-7 show a general agreement between the model results and the KG-1-CP observations, although the correspondence being a bit lower in the extra campaign period.

The overall conclusion from this reverification is that the quality of the 3D current model results is consistent throughout the whole campaign period.

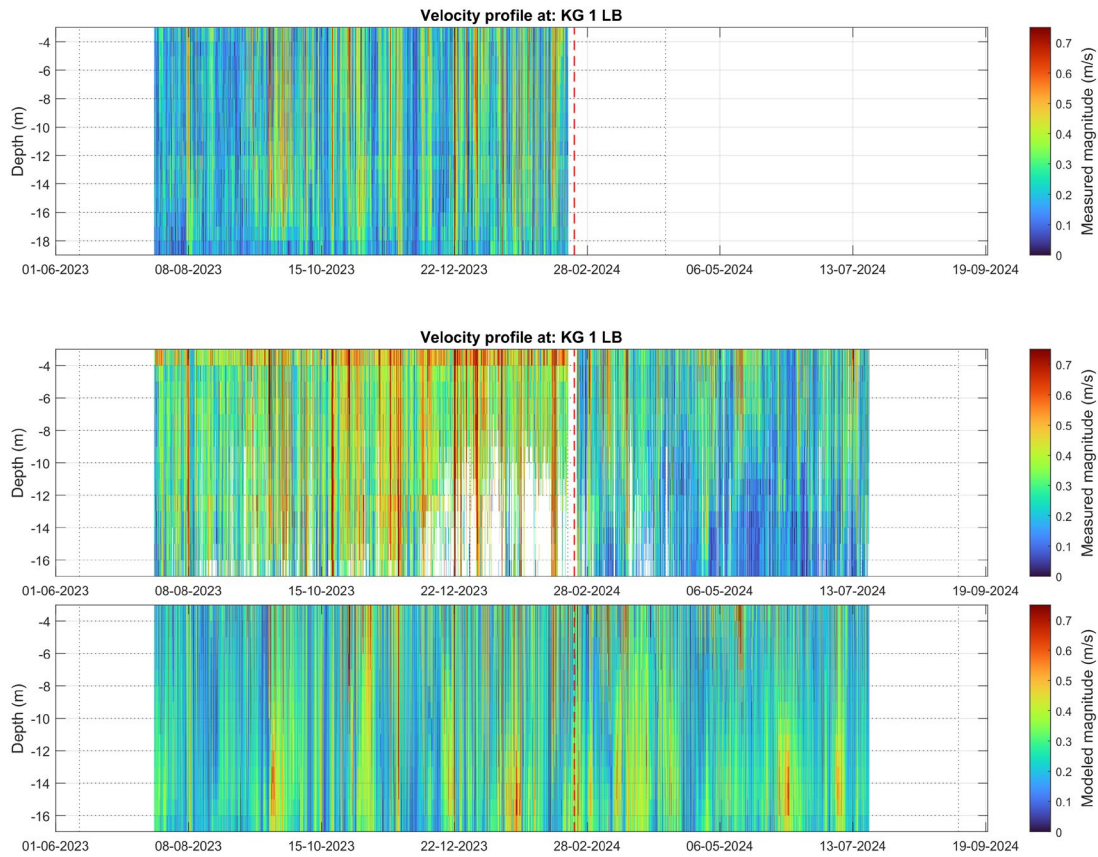
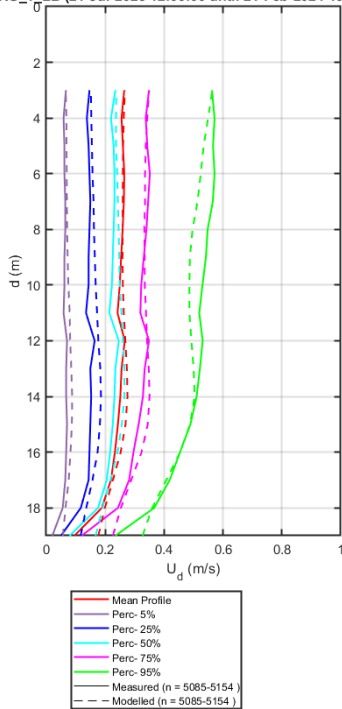


Figure 6-4 Current speed Hovmöller diagrams of the calibrated model results and the observations from KG-1-LB. The plot in the top row is with the observations considered in Deltares (2024), the plot in the bottom row is with the final campaign observations and the plot in the bottom row is with the model results.

KG_1_LB (21-Jul-2023 12:00:00 until 21-Feb-2024 10:00:00)



KG_1_LB (21-Jul-2023 12:00:00 until 21-Feb-2024 10:00:00) KG_1_LB (21-Feb-2024 11:00:00 until 21-Jul-2024 11:00:00) KG_1_LB (21-Jul-2023 12:00:00 until 21-Jul-2024 11:00:00)

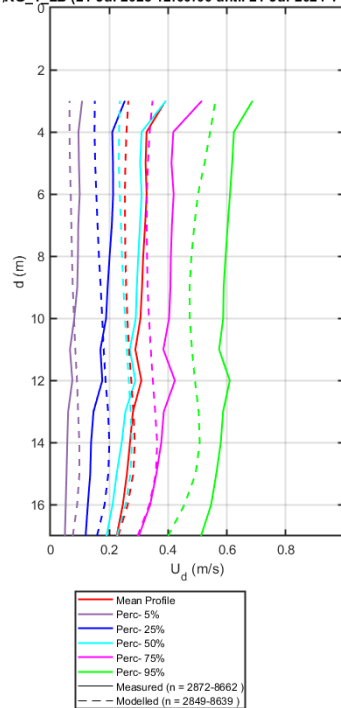
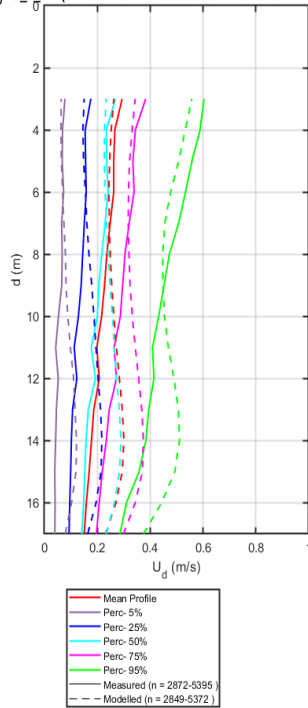
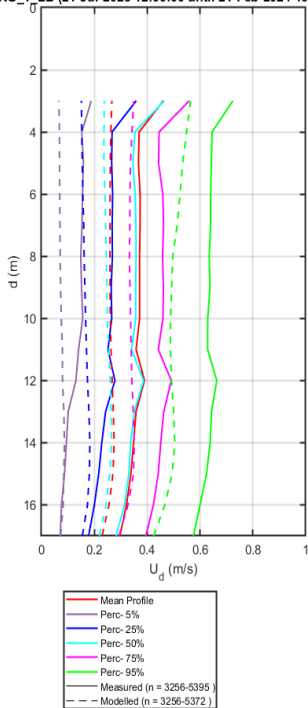


Figure 6-5 Current magnitude 3D profile plots comparisons between the calibrated 3D model results (dashed lines) and the observations (full lines) from KG-1-LB. The plot in the top row is for the observations considered in Deltares (2024), the plots in the bottom row are for the final campaign observations. The periods covered by the data are 07-2023 to 03-2024 (left column), 03-2024 to 07-2024 (middle column) and 07-2023 to 07-2024 (right column).

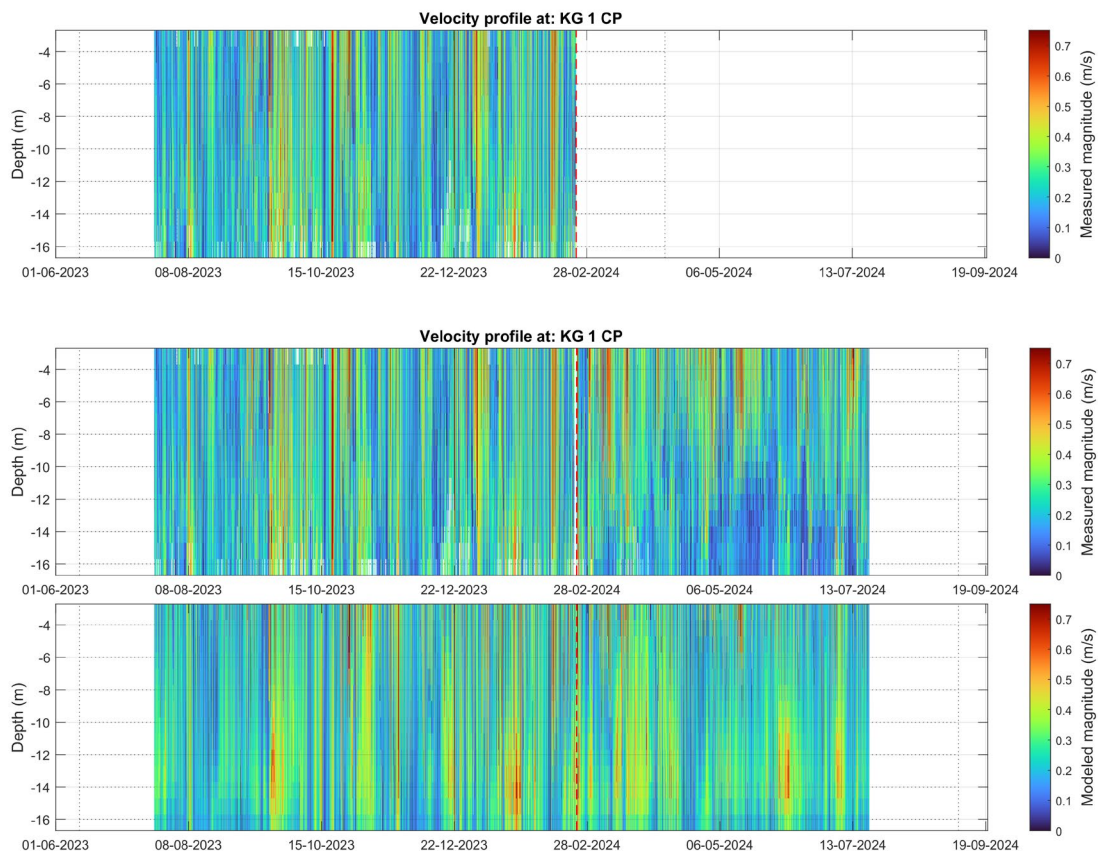
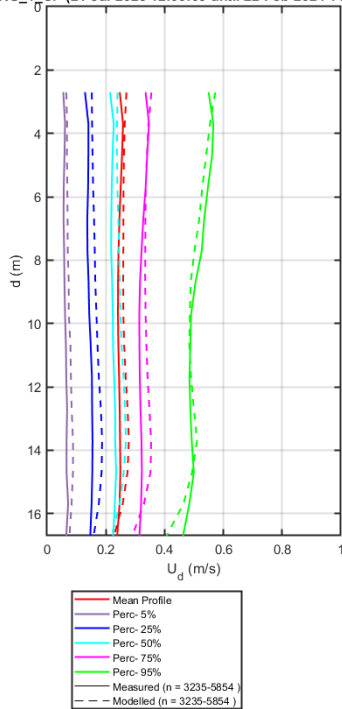


Figure 6-6 Current speed Hovmöller diagrams of the calibrated model results and the observations from KG-1-CP. The plot in the top row is with the observations considered in Deltares (2024), the plot in the bottom row is with the final campaign observations and the plot in the bottom row is with the model results.

KG_1_CP (21-Jul-2023 12:00:00 until 22-Feb-2024 14:00:00)



KG_1_CP (21-Jul-2023 12:00:00 until 22-Feb-2024 14:00:00) KG_1_CP (22-Feb-2024 15:00:00 until 21-Jul-2024 11:00:00) KG_1_CP (21-Jul-2023 12:00:00 until 21-Jul-2024 11:00:00)

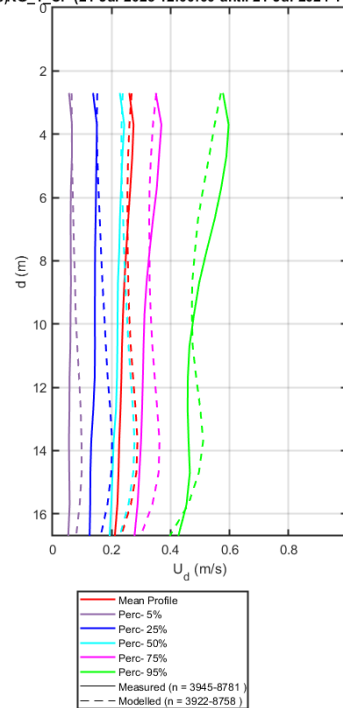
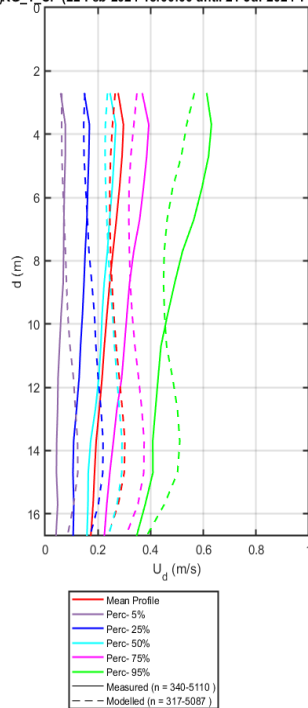
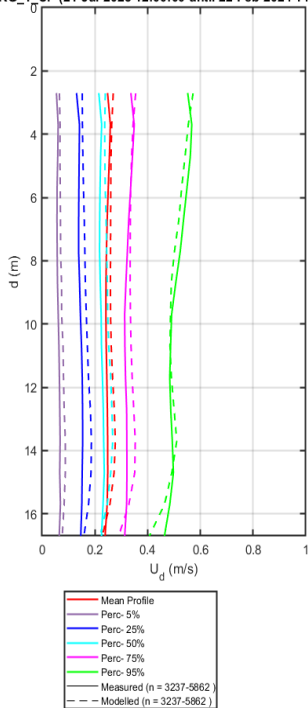


Figure 6-7 Current magnitude 3D profile plots comparisons between the calibrated 3D model results (dashed lines) and the observations (full lines) from KG-1-CP. The plot in the top row is for the observations considered in Deltares (2024), the plots in the bottom row are for the final campaign observations. The periods covered by the data are 07-2023 to 03-2024 (left column), 03-2024 to 07-2024 (middle column) and 07-2023 to 07-2024 (right column).

6.3 Hesselø South currents

Figure 6-8 shows the timeseries comparisons between the depth-averaged current speed model results and observations from HS-1-LB and HS-1-CP. The respective density scatter comparisons are given in Figure 6-9 for HS-1-LB and Figure 6-10 for HS-1-CP.

There is no final campaign data from HS-1-LB in the period considered in Deltares (2024) and the correspondence between the model results and the data considered in Deltares (2024) and the final campaign data is comparable (Figure 6-9). The correspondence between the model results and the observations from HS-1-CP considered in Deltares (2024) and the final HS-1-CP campaign data is also comparable.

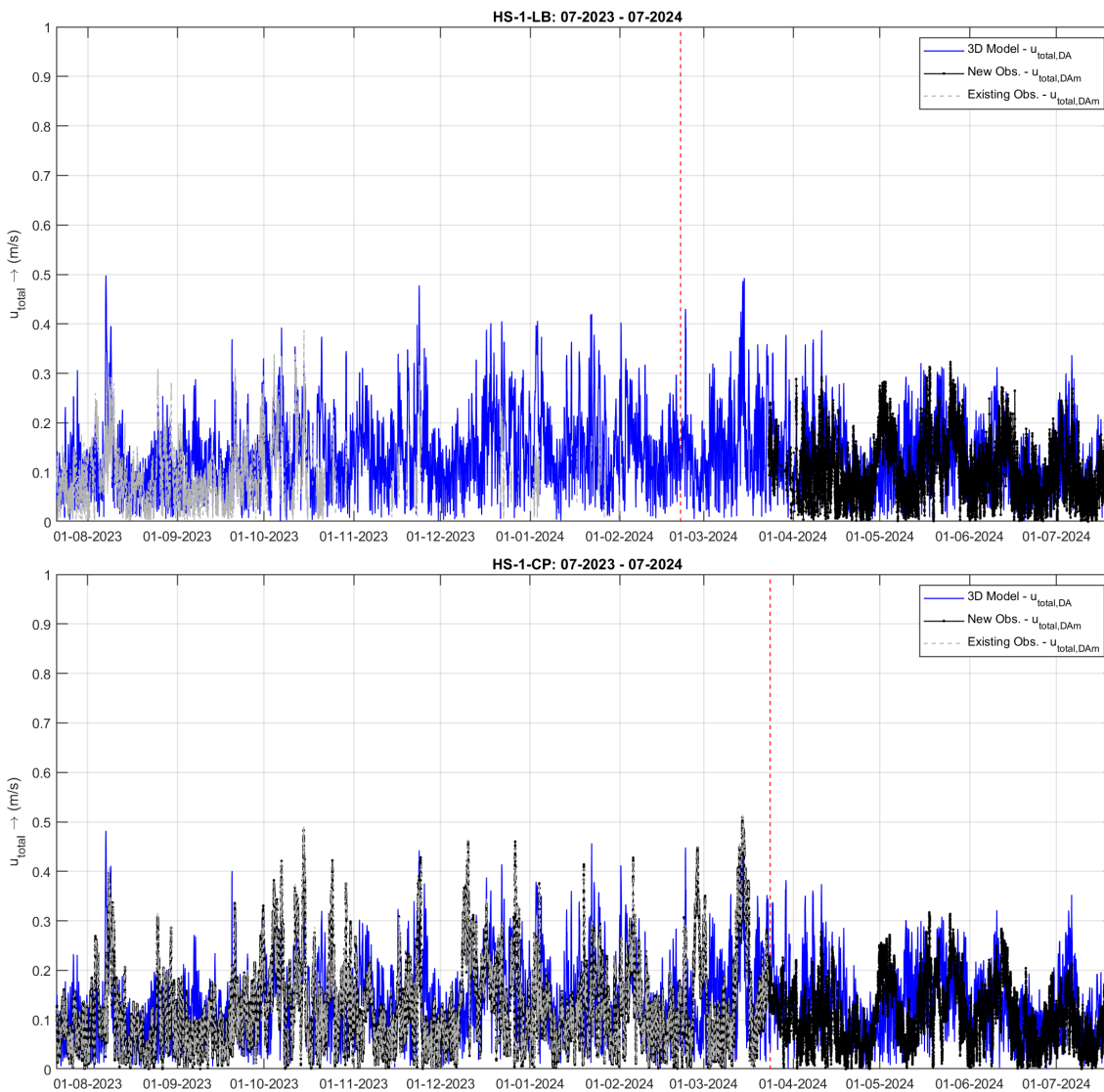


Figure 6-8 Timeseries comparisons between the calibrated model results and the observations from HS-1-LB (top) and HS-1-CP (bottom) of depth-averaged current speed.

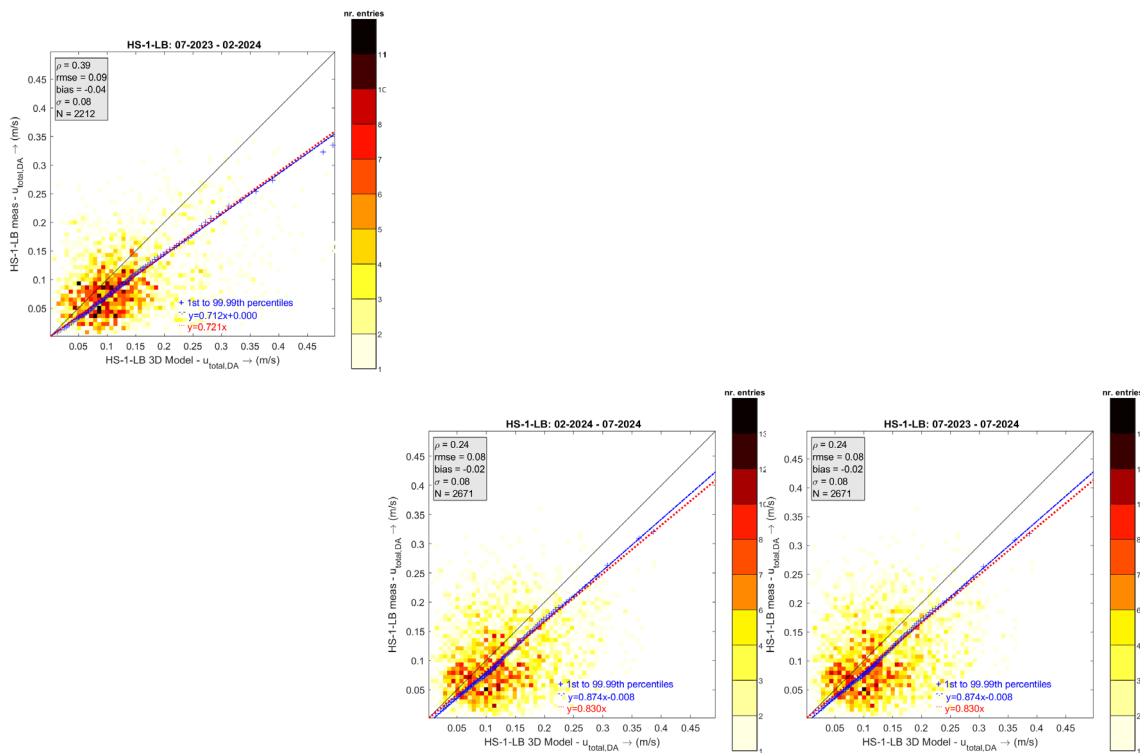


Figure 6-9 Density scatter comparisons between the calibrated 3D model results and the observations from HS-1-LB of depth-averaged current speed. The plot in the top row is for the observations considered in Deltares (2024), the plots in the bottom row are for the final campaign observations. The periods covered by the data are 07-2023 to 02-2024 (left column, no valid data in the final campaign dataset), 02-2024 to 07-2024 (middle column) and 07-2023 to 07-2024 (right column).

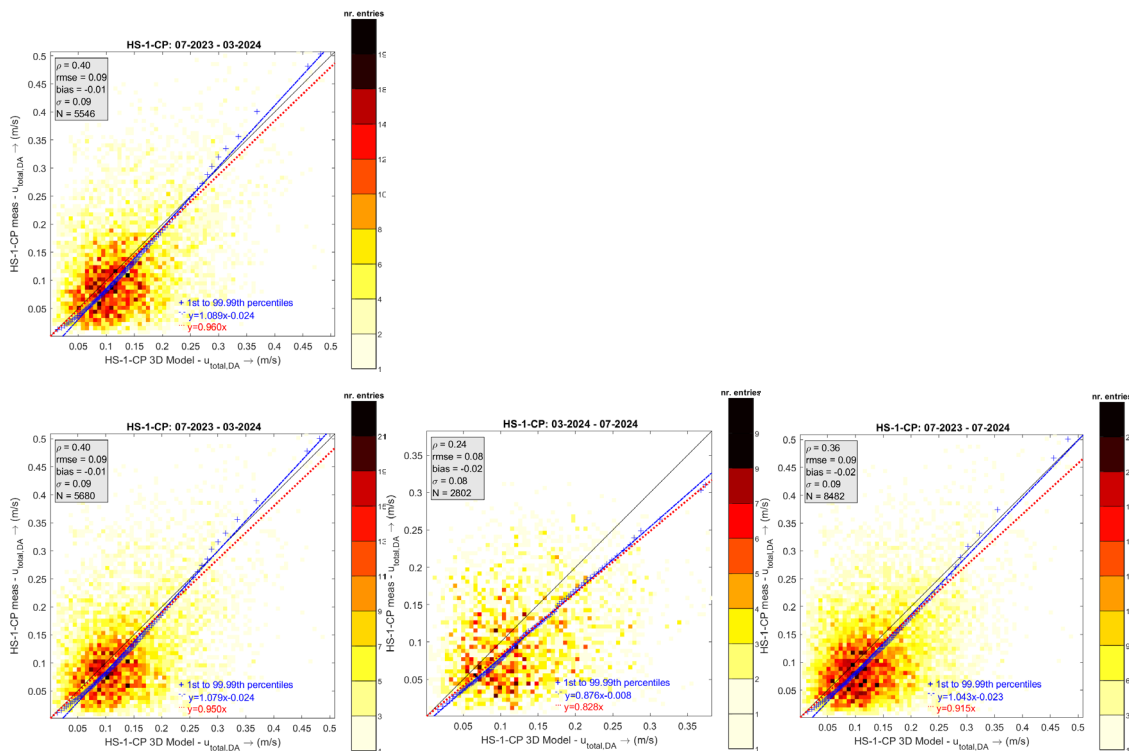


Figure 6-10 Density scatter comparisons between the calibrated 3D model results and the observations from HS-1-CP of depth-averaged current speed. The plot in the top row is for the observations considered in Deltares (2024), the plots in the bottom row are for the final campaign observations. The periods covered by the data are 07-2023 to 03-2024 (left column), 03-2024 to 07-2024 (middle column) and 07-2023 to 07-2024 (right column).

Figure 6-11 shows the Hovmöller diagrams of the HS-1-LB current speed observations considered in Deltares (2024), the final campaign observations and the calibrated 3D model results and Figure 6-12 shows the respective HS-1-LB vertical current speed profile plot comparisons. Figure 6-13 and Figure 6-14 show respectively the Hovmöller diagrams and the vertical current speed profile plot comparisons of the HS-1-CP current speed observations considered in Deltares (2024), the final campaign observations and the calibrated 3D model results. As also shown in the depth-averaged current speed comparisons, the correspondence between the model results and the observations from HS-1-LB and HS-1-CP in the period considered in Deltares (2024) and the total (final) HS-1-LB and HS-1-CP campaign period is comparable.

The overall conclusion from this reverification is that the quality of the 3D current model results is consistent throughout the whole campaign period.

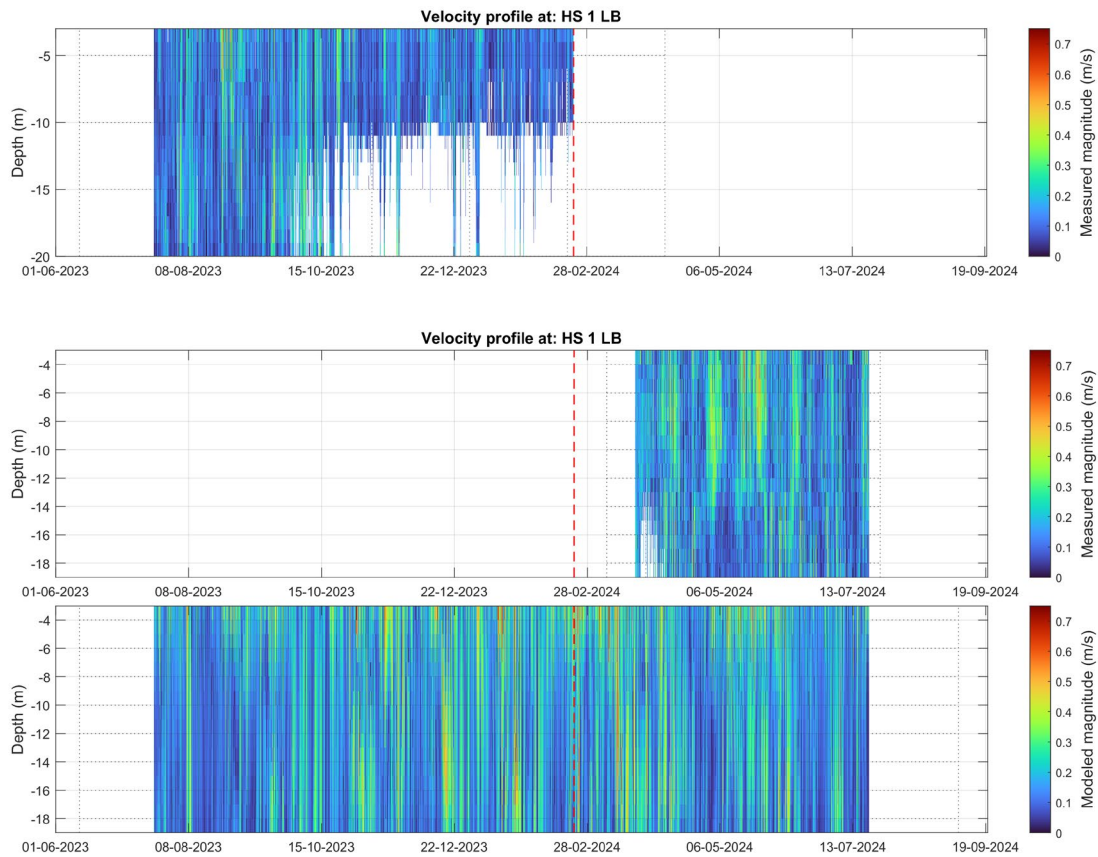
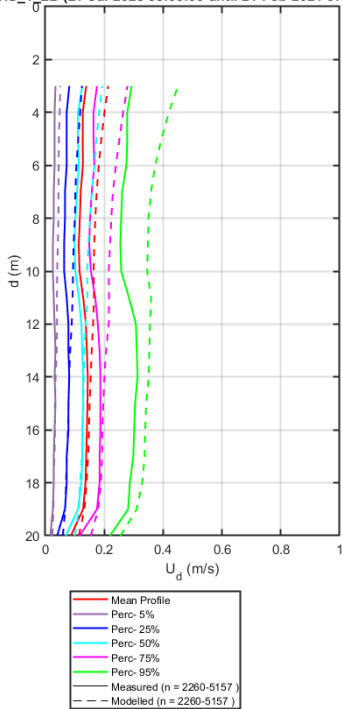


Figure 6-11 Current speed Hovmöller diagrams of the calibrated model results and the observations from HS-1-LB. The plot in the top row is with the observations considered in Deltares (2024), the plot in the bottom row is with the final campaign observations and the plot in the bottom row is with the model results.

HS_1_LB (21-Jul-2023 08:00:00 until 21-Feb-2024 07:00:00)



HS_1_LB (21-Feb-2024 08:00:00 until 21-Jul-2024 07:00:00) HS_1_LB (21-Jul-2023 08:00:00 until 21-Jul-2024 07:00:00)

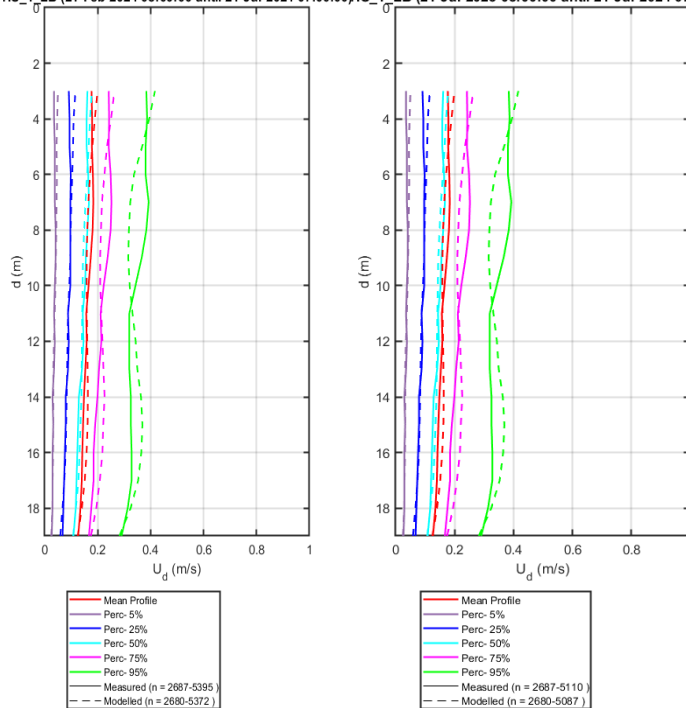


Figure 6-12 Current magnitude 3D profile plots comparisons between the calibrated 3D model results (dashed lines) and the observations (full lines) from HS-1-LB. The plot in the top row is for the observations considered in Deltares (2024), the plots in the bottom row are for the final campaign observations. The periods covered by the data are 07-2023 to 03-2024 (left column, no valid data in the final campaign dataset), 03-2024 to 07-2024 (middle column) and 07-2023 to 07-2024 (right column).

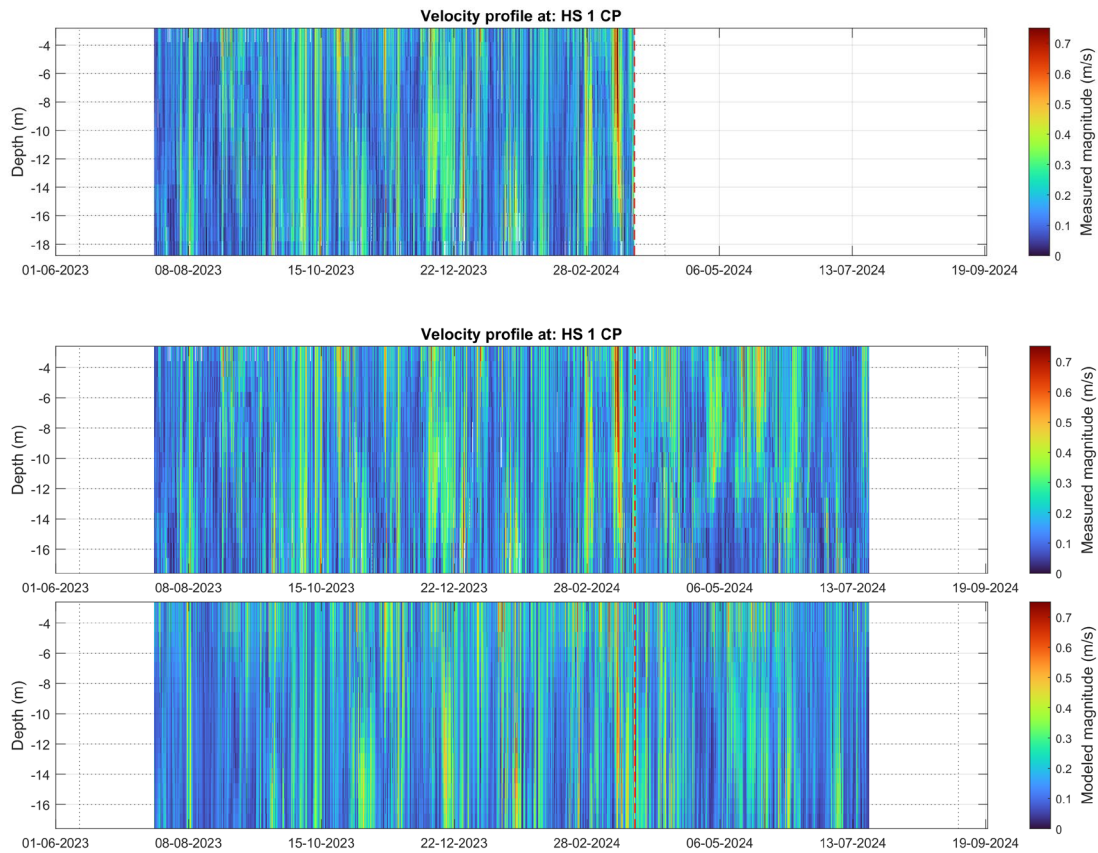
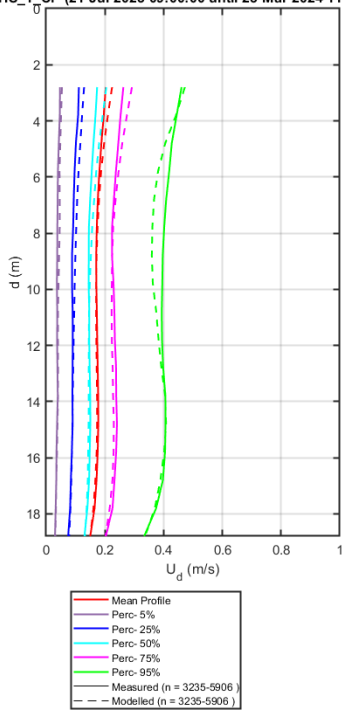


Figure 6-13 Current speed Hovmöller diagrams of the calibrated model results and the observations from HS-1-CP. The plot in the top row is with the observations considered in Deltares (2024), the plot in the bottom row is with the final campaign observations and the plot in the bottom row is with the model results.

HS_1_CP (21-Jul-2023 09:00:00 until 23-Mar-2024 11:00:00)



HS_1_CP (21-Jul-2023 09:00:00 until 23-Mar-2024 11:00:00) HS_1_CP (23-Mar-2024 12:00:00 until 21-Jul-2024 07:00:00) HS_1_CP (21-Jul-2023 09:00:00 until 21-Jul-2024 07:00:00)

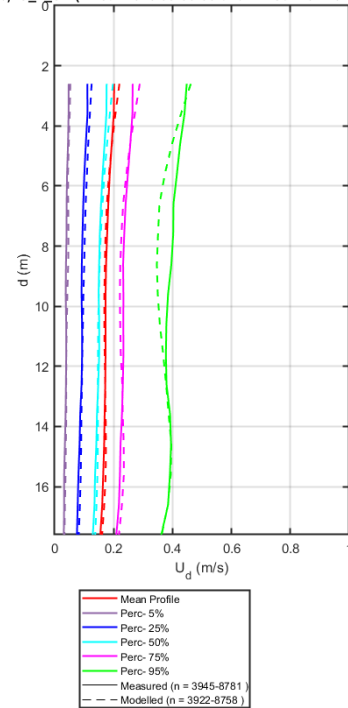
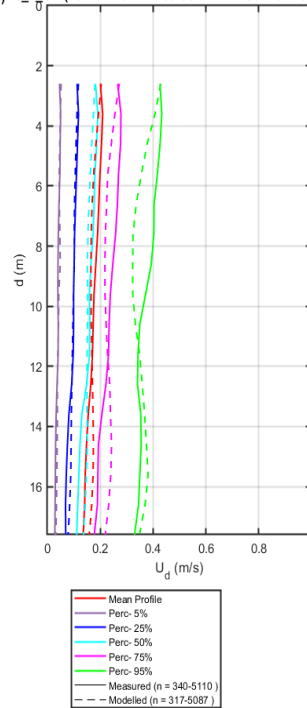
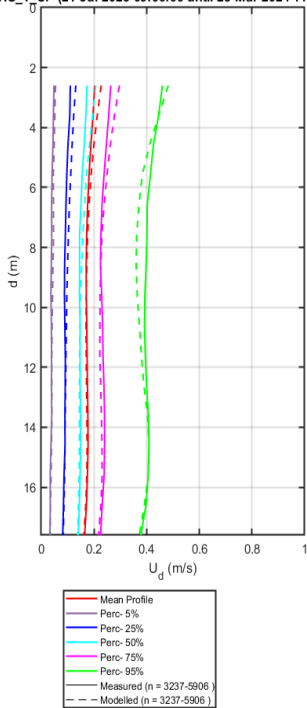


Figure 6-14 Current magnitude 3D profile plots comparisons between the calibrated 3D model results (dashed lines) and the observations (full lines) from HS-1-CP. The plot in the top row is for the observations considered in Deltares (2024), the plots in the bottom row are for the final campaign observations. The periods covered by the data are 07-2023 to 03-2024 (left column), 03-2024 to 07-2024 (middle column) and 07-2023 to 07-2024 (right column).

7 Temperature reverification

7.1 Kattegat and Hesselø South water temperature

The validation of thermodynamic parameters was performed in Deltares (2024) using KG-1-CP near-bottom temperature observations, the KG-1-LB near-surface temperature observations and HS-1-CP near-bottom temperature observations. New data are now available from KG-1-LB, KG-1-CP, HS-1-LB and HS-1-CP. Figure 7-1 and Figure 7-2 show the comparisons at KG and HS, respectively, considering the observations from the full campaign period (Fugro, 2024a,b). The figures show that there is a general agreement between the model results and the observations in both periods, indicating that the assessed validity of thermodynamic 3D model results in Deltares (2024) still holds.

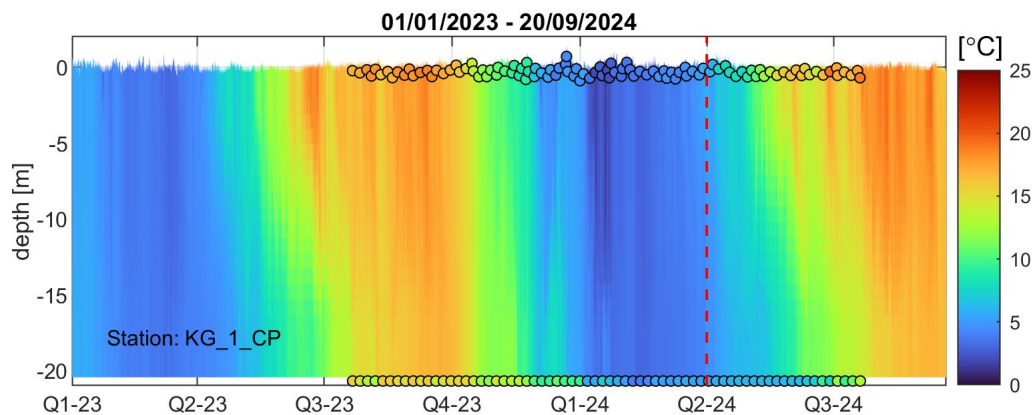


Figure 7-1 Hovmöller diagrams of the 3D temperature model results (background colour map) and near-bottom and near-surface temperature observations (coloured circles) from KG-1-CP and KG-1-LB, respectively. The vertical line indicates the date until which the observation data have been considered in the Deltares (2024).

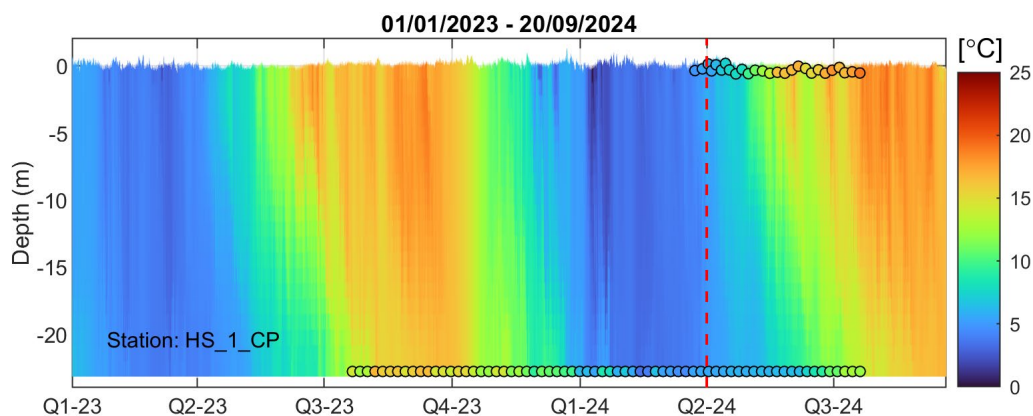


Figure 7-2 Hovmöller diagrams of the 3D temperature model results (background colour map) and near-bottom and near-surface temperature observations (coloured circles) from HS-1-CP and HS-1-LB, respectively. The vertical line indicates the date until which the observation data have been considered in the Deltares (2024).

8 Wave reverification

8.1 Introduction

The following sections 8.2 and 8.3 show the comparisons between the calibrated model results and the observations of significant wave height (H_s), peak wave period (T_p) and mean wave direction (MWD) from KS-1 and HS-1, respectively.

8.2 Kattegat waves

Figure 8-1 shows the timeseries comparisons between the model results and the observations of H_s , T_p and MWD at KG-1-LB. The respective density scatter comparisons are given in Figure 8-2. The figures show that the correspondence between the model results and the KG-1-LB observations is similar in the considered periods, with comparable correlation and fit coefficients. It is, therefore, concluded that the quality of the wave model data is consistent throughout the whole campaign period.

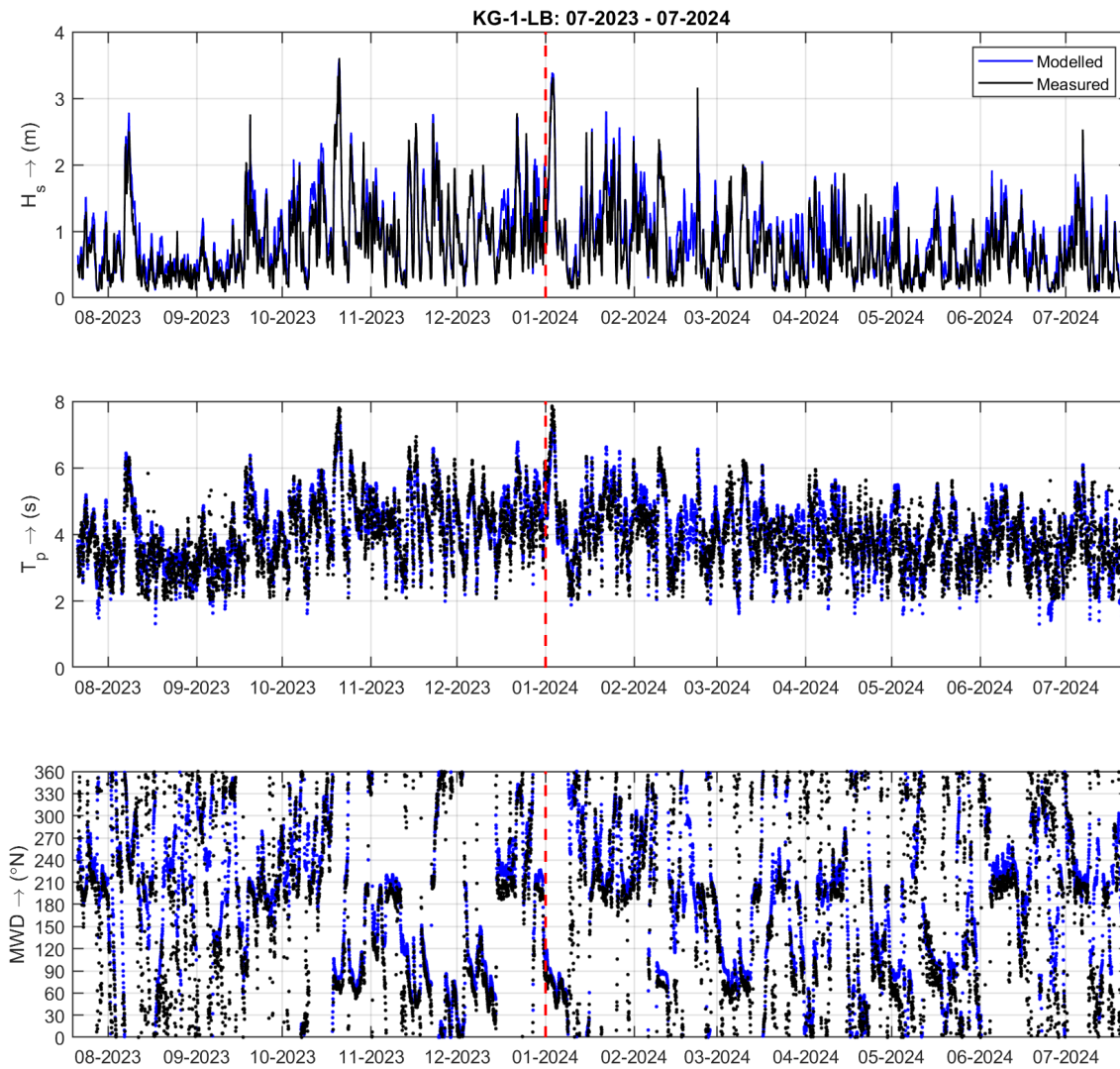


Figure 8-1 Timeseries comparisons between the calibrated model results and the observations from KG-1-LB of significant wave height (top panel), peak wave period (middle panel) and mean wave direction (bottom panel). The vertical line indicates the date until which the observation data have been considered in the Deltares (2024).

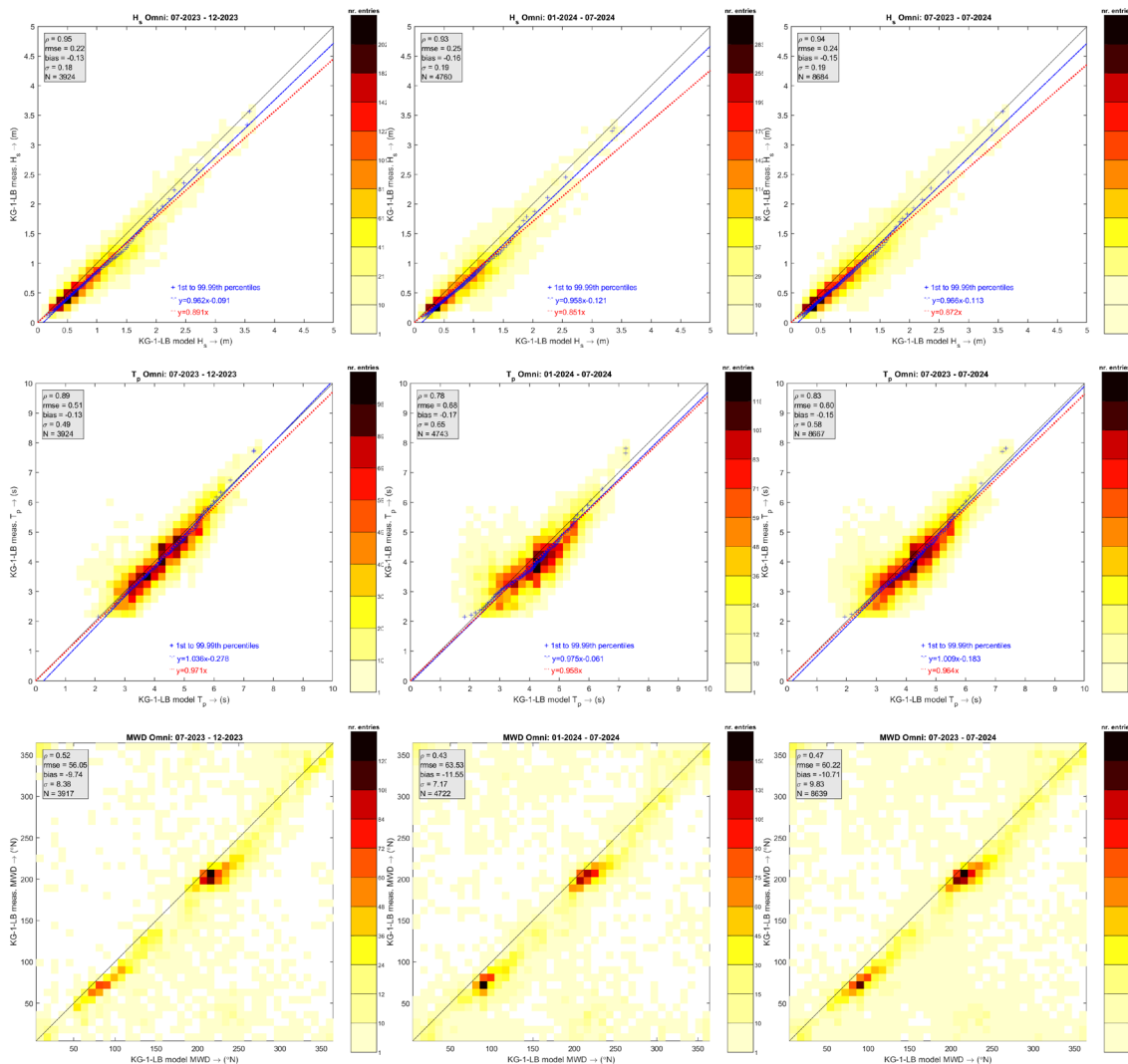


Figure 8-2 Density scatter comparisons between the calibrated model results and the observations from KG-1-LB of significant wave height (top row), peak wave period (middle row) and mean wave direction (bottom row). The periods covered by the data are 07-2023 to 12-2023 (left column), 01-2024 to 07-2024 (middle column) and 07-2023 to 07-2024 (right column).

8.3 Hesselø South waves

Figure 8-3 shows the timeseries comparisons between the model results and the observations of H_s , T_p and MWD at HS-1-LB. The respective density scatter comparisons are given in Figure 8-4. The figures show that the correspondence between the model results and the HS-1-LB observations is similar in the considered periods, with comparable correlation and fit coefficients, although the overestimation of the observations by the model results is slightly higher in the campaign period not considered in Deltares (2024), from 01-2024 to 07-2024. It can, nevertheless be concluded that the quality of the wave model data is consistent throughout the whole campaign period.

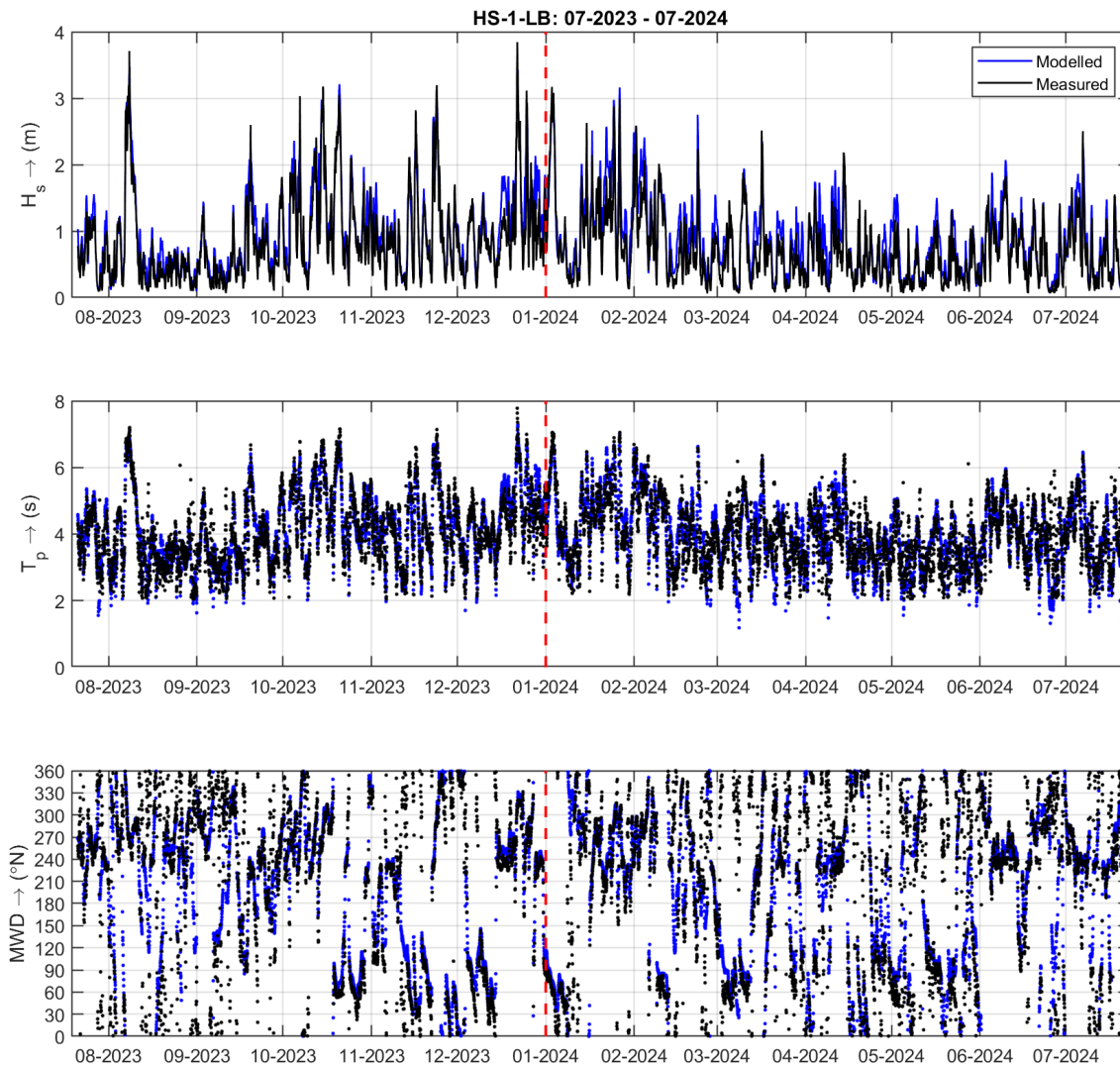


Figure 8-3 Timeseries comparisons between the calibrated model results and the observations from HS-1-LB of significant wave height (top panel), peak wave period (middle panel) and mean wave direction (bottom panel). The vertical line indicates the date until which the observation data have been considered in the Deltares (2024).

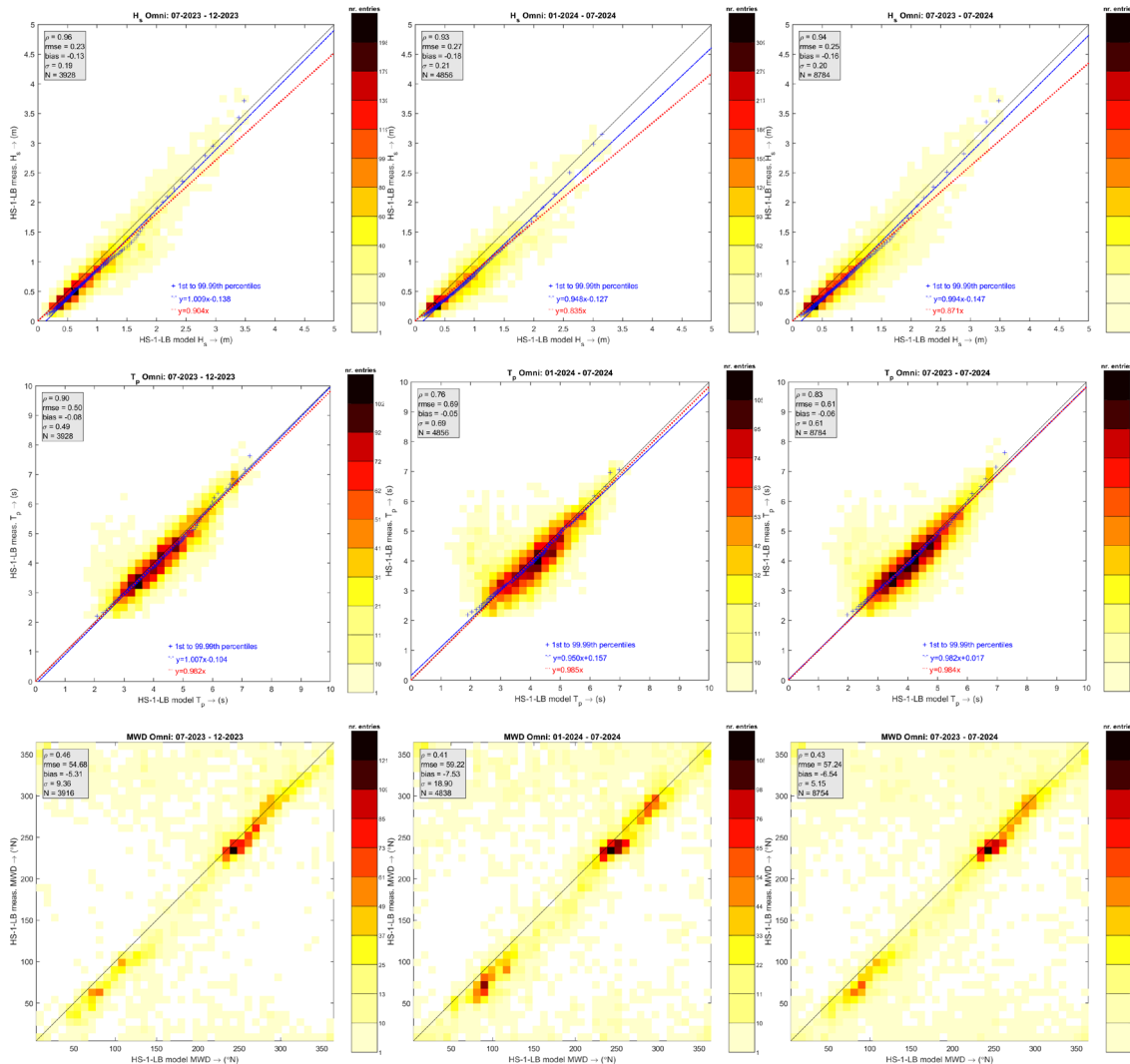


Figure 8-4 Density scatter comparisons between the calibrated model results and the observations from HS-1-LB of significant wave height (top row), peak wave period (middle row) and mean wave direction (bottom row). The periods covered by the data are 07-2023 to 12-2023 (left column), 01-2024 to 07-2024 (middle column) and 07-2023 to 07-2024 (right column).

9 References

- Deltares, 2024: Kattegat and Hesselø South Site Metocean Conditions Assessments, Part A: Measurements and Hindcast Data Basis, dated 15-10-2024 (KGHS_Report_PartA_for_ENDK-SWECO_rev2 - signed.pdf).
- Fugro, 2024a: Danish Offshore Wind 2030 – Floating LiDAR Measurements: Final Campaign Report for Kattegat, July 2023 – July 2024, C75516-R12-KG-001 02, dated: 25-09-2024 (C75516-R12-KG-001(02)-Final Report.pdf).
- Fugro, 2024b: Danish Offshore Wind 2030 – Floating LiDAR Measurements: Final Campaign Report for Hesselø South, July 2023 – July 2024, C75516-R12-HS-001 02, dated: 8-10-2024 (C75516-R12-HS-001(02)-Final Report.pdf).
- SWECO, 2024a: Kattegat and Hesselø South Site MetOcean Conditions Assessments: Part B: Analyses and Design Parameters for Kattegat (41011328B_KG_PartB_Analyses_and_Design_Parameters).
- SWECO, 2024b: Kattegat and Hesselø South Site MetOcean Conditions Assessments: Part C: Analyses and Design Parameters for Hesselø South (41011328C_HS_PartC_Analyses_and_Design_Parameters).

Appendix A Error statistics

Introduction

A particularity of certain environmental data (e.g. wave data) is that they can be classified into *linear data* (e.g. mean wave period and significant wave height) and *circular data* (e.g. mean wave direction and directional spread), and this distinction must be taken into consideration when carrying out error analysis (Van Os and Caires, 2011). The statistical techniques for dealing with these two types of data are different – circular (or directional) data require a special approach. Basic concepts of statistical analysis of circular data are given in the books of Mardia (1972) and Fisher (1993).

Linear variables

Differences between linear variables are often quantified using the following standard statistics:

- the bias: $\bar{y} - \bar{x}$;
- the root-mean-square error: $RMSE = \sqrt{n^{-1} \sum (y_i - x_i)^2}$;
- the scatter index: $SI = \frac{\sqrt{n^{-1} \sum [(y_i - \bar{y}) - (x_i - \bar{x})]^2}}{\bar{x}}$;
- the correlation coefficient: $\rho = \frac{\sum [(x_i - \bar{x}) - (y_i - \bar{y})]}{\sqrt{\sum (x_i - \bar{x})^2 \sum (y_i - \bar{y})^2}}$;
- the symmetric slope: $r = \sqrt{\sum x_i^2 / \sum y_i^2}$.

In all these formulae x_i usually represents observations (or the dataset which is considered less uncertain or baseline), y_i represents the model results (or the dataset which is considered more uncertain or with a certain deviation from the baseline results) and n the number of observations. In this study, when trying to derive calibration expressions, x_i corresponds to the model results.

Circular variables

If we compute an average of angles as their arithmetic mean, we may find that the result is of little use as a statistical location measure. Consider for instance the case of two angles of 359° and 1°; their arithmetic mean is 180°, when in reality 359° is only two degrees away from 1° and the mid direction between the two is 0°. This phenomenon is typical for circular data and illustrates the need for special definitions of statistical measures in general.

When dealing with circular data, each observation is considered as unit vector, and it requires vector addition rather than ordinary (or scalar) addition to compute the average of angles, the so-called mean direction.

Writing

$$C_n = \sum_{i=1}^n \cos x_i \quad \text{and} \quad S_n = \sum_{i=1}^n \sin x_i, \quad (\text{A.1})$$

the *sample resultant vector* R_n of a sample $x = \{x_i, i = 1, \dots, n\}$ is defined as

$$R_n = \sqrt{C_n^2 + S_n^2},$$

and its *sample mean direction* $\bar{x} \equiv \bar{x}_n$ as the direction of R_n :

$$\bar{x} = \text{TAN}^{-1}(S_n/C_n) \quad (\text{A.2})$$

where $\text{TAN}^{-1}(S_n/C_n)$ is the inverse of the tangent of (S_n/C_n) in the range $[0, 2\pi [$, i.e.,

$$\text{TAN}^{-1}\left(\frac{S_n}{C_n}\right) = \begin{cases} \tan^{-1}\left(\frac{S_n}{C_n}\right), & S_n > 0, C_n > 0 \\ \tan^{-1}\left(\frac{S_n}{C_n}\right) + \pi, & C_n < 0 \\ \tan^{-1}\left(\frac{S_n}{C_n}\right) + 2\pi, & S_n < 0, C > 0. \end{cases}$$

The *sample mean resultant length* of $x = \{x_i, i = 1, \dots, n\}$ is defined by

$$\bar{R}_n = R_n / n, 0 < \bar{R}_n < 1$$

If $\bar{R}_n = 1$, then all angles coincide.

Eq. (A.2) can be used to compute the bias between two circular variables by substituting x_i by $y_i - x_i$ in Eq. (A.1). In a similar way, the root-mean-square error and standard deviation between two circular variables can be computed.

Since circular data are concentrated on $[0^\circ, 360^\circ]$, and in spite of the analogies with the linear case, it makes no sense to consider a symmetric slope for circular data other than one.

There are several circular analogues of the correlation coefficient, but the most widely used is the one proposed by Fisher and Lee (1983), the so-called *T-linear correlation coefficient*. Given two sets $x = \{x_i, i = 1, \dots, n\}$, $y = \{y_i, i = 1, \dots, n\}$ of circular data, the *T-linear correlation coefficient* between x and y is defined by

$$\rho_T = \frac{\sum_{1 \leq i < j \leq n} \sin(x_i - x_j) \sin(y_i - y_j)}{\sqrt{\sum_{1 \leq i < j \leq n} \sin^2(x_i - x_j) \sum_{1 \leq i < j \leq n} \sin^2(y_i - y_j)}}.$$

This statistic satisfies $-1 \leq \rho_T \leq 1$, and its population counterpart (which is not given here but can be seen in Fisher and Lee, 1983) satisfies properties analogous to those of the usual population correlation coefficient for linear data: that is, the population counterpart achieves the extreme values -1 and 1 if and only if the two population variables involved are exactly 'T-linear associated', with the sign indicating discordant or concordant rotation, respectively (see Fisher (1993), p. 146, for these concepts).

For computational ease, we use an equivalent formula for ρ_T , given by Fisher (1993):

$$\rho_T = \frac{4(AB-CD)}{\sqrt{(n^2-E^2-F^2)}\sqrt{(n^2-G^2-H^2)}}$$

where

$$A = \sum_{i=1}^n \cos x_i \cos y_i, \quad B = \sum_{i=1}^n \sin x_i \sin y_i,$$

$$C = \sum_{i=1}^n \cos x_i \sin y_i, \quad D = \sum_{i=1}^n \sin x_i \cos y_i,$$

$$E = \sum_{i=1}^n \cos(2x_i), \quad F = \sum_{i=1}^n \sin(2x_i),$$

$$G = \sum_{i=1}^n \cos(2y_i), \quad H = \sum_{i=1}^n \sin(2y_i).$$

References

Fisher, N.I., 1993. Statistical analysis of circular data. Cambridge Univ. Press, 277 pp.

Fisher, N.I. and A.J. Lee, 1983. A correlation coefficient for circular data. Biometrika, 70, pp. 327-32.

Mardia, K.V., 1972. Statistics of directional data. Academic Press, (London and New York).

Van Os, J. and S. Caires, 2011: How to Carry out metocean studies. Proc. 30th Int. Conf. on Offshore Mechanics and Arctic Eng. (OMAE2011-49066).

Together with our clients and the collective knowledge of our 22,000 architects, engineers and other specialists, we co-create solutions that address urbanisation, capture the power of digitalisation, and make our societies more sustainable.

Sweco – Transforming society together